ORTA DOĞU TEKNİK ÜNİVERSİTESİ
FEN BİLİMLERİ ENSTİTÜSÜ MÜDÜRLÜĞÜ

TEZ ŞABLONU ONAY FORMU
THESIS TEMPLATE CONFIRMATION FORM

1. Şablonda verilen yerleşim ve boşluklar değiştirilmemelidir.
2. Jüri tarihi Başlık Sayfası, İmza Sayfası, Abstract ve Öz'de ilgili yerlere yazılmalıdır.
3. İmza sayfasında jüri üyelerinin unvanları doğru olarak yazılmalıdır.
4. Tezin son sayfasının sayfa numarası Abstract ve Öz'de ilgili yerlere yazılmalıdır.
5. Bütün chapterlar, referanslar, ekler ve CV sağ sayfada başlamalıdır. Bunun için **kesmeler** kullanılmıştır. **Kesmelerin kayması** fazladan boş sayfaların oluşmasına sebep olabilir. Bu gibi durumlarda paragraf (¶) işaretine tıklayarak kesmeleri görünür hale getirin ve yerlerini **kontrol edin**.
6. Figürler ve tablolar kenar boşluklarına taşmamalıdır.
7. Şablonda yorum olarak eklenen uyarılar dikkatle okunmalı ve uygulanmalıdır.
8. Tez yazdırılmadan önce PDF olarak kaydedilmelidir. Şablonda yorum olarak eklenen uyarılar PDF dokümanında yer almamalıdır.
9. **Bu form aracılığıyla oluşturulan PDF dosyası arkalı-önlü baskı alınarak tek bir spiralli cilt haline getirilmelidir.**
10. Spiralli hale getirilen tez taslağınızdaki ilgili alanları imzalandıktan sonra, Tez Juri Atama Formu ile birlikte bölüm sekreterliğine teslim edilmelidir.
11. Tez taslağınız bölüm sekreterliğiniz aracılığıyla format ve görünüm açısından kontrol edilmek üzere FBE'ye ulaştırılacaktır.
12. FBE tarafından kontrol işlemleri tamamlanan tez taslakları, öğrencilere teslim edilmek üzere bölüm sekreterliklerine iletilecektir.
13. Tez taslaklarının kontrol işlemleri tamamlandığında, bu durum öğrencilere METU uzantılı öğrenci e-posta adresleri aracılığıyla duyurulacaktır.
14. Tez taslakları bölüm sekreterlikleri tarafından öğrencilere iletileceği için öğrencilerimizin tez taslaklarını enstitümüzden elden alma konusunda ısrarcı olmamaları beklenmektedir.
15. Tez yazım süreci ile ilgili herhangi bir sıkıntı yaşarsanız, **Sıkça Sorulan Sorular (SSS)** sayfamızı ziyaret ederek yaşadığınız sıkıntıyla ilgili bir çözüm bulabilirsiniz.

1. Do not change the spacing and placement in the template.
2. Write defense date to the related places given on Title page, Approval page, Abstract and Öz.
3. Write the titles of the examining committee members correctly on Approval Page.
4. Write the page number of the last page in the related places given on Abstract and Öz pages.
5. All chapters, references, appendices and CV must be started on the right page. **Section Breaks** were used for this. **Change in the placement** of section breaks can result in extra blank pages. In such cases, make the section breaks visible by clicking paragraph (¶) mark and **check their position.**
6. All figures and tables must be given inside the page. Nothing must appear in the margins.
7. All the warnings given on the comments section through the thesis template must be read and applied.
8. Save your thesis as pdf and Disable all the comments before taking the printout.
9. **Print two-sided the PDF file that you have created through this form and make a single spiral bound.**
10. Once you have signed the relevant fields in your thesis draft that you spiraled, submit it to the department secretary together with your Thesis Jury Assignment Form.
11. Your thesis draft will be delivered to the GSNAS via your department secretary for controlling in terms of format and appearance.
12. The thesis drafts that are controlled by GSNAS, will be sent to the department secretary to be delivered to the students.
13. This will be announced to the students via their METU students e-mail addresses when the control of the thesis drafts has been completed.
14. As the thesis drafts will be delivered to the students by the department secretaries, we are expecting from our students no to insist about getting their theses drafts from the Institute.
15. If you have any problems with the thesis writing process, you may visit our **Frequently Asked Questions (FAQ)** page and find a solution to your problem.

☒ **Yukarıda bulunan tüm maddeleri okudum, anladım ve kabul ediyorum. / I have read, understand and accept all of the items above.**

Name :
Surname :
E-Mail :
Date :
Signature : ________________________

SUPPRESSION OF TOOL TIP FRF IN MACHINE TOOL ASSEMBLIES BY COMPONENT MODE TUNING METHOD

A THESIS SUBMITTED TO
THE GRADUATE SCHOOL OF NATURAL AND APPLIED SCIENCES
OF
MIDDLE EAST TECHNICAL UNIVERSITY

BY

GAMZE KARATAŞ

IN PARTIAL FULFILLMENT OF THE REQUIREMENTS
FOR
THE DEGREE OF MASTER OF SCIENCE
IN
MECHANICAL ENGINEERING

SEPTEMBER 2020

Approval of the thesis:

SUPPRESSION OF TOOL TIP FRF IN MACHINE TOOL ASSEMBLIES BY COMPONENT MODE TUNING METHOD

submitted by **GAMZE KARATAŞ** in partial fulfillment of the requirements for the degree of **Master of Science** in **Mechanical Engineering, Middle East Technical University** by,

Prof. Dr. Halil Kalıpçılar
Dean, Graduate School of **Natural and Applied Sciences** ________________

Prof. Dr. M.A. Sahir Arıkan
Head of the Department, **Mechanical Engineering** ________________

Prof. Dr. H. Nevzat Özgüven
Supervisor, **Mechanical Engineering, METU** ________________

Prof. Dr. Erhan Budak
Co-Supervisor, **Fac. of Eng. and Natural Sci., Sabancı Uni.** ________________

Examining Committee Members:

Assoc. Prof. Dr. M. Bülent Özer
Mechanical Engineering, METU ________________

Prof. Dr. H. Nevzat Özgüven
Mechanical Engineering, METU ________________

Assist. Prof. Dr. Gökhan Özgen
Mechanical Engineering, METU ________________

Assist. Prof. Dr. Orkun Özşahin
Mechanical Engineering, METU ________________

Prof. Dr. Erhan Budak
Fac. of Eng. and Natural Sci., Sabancı Uni. ________________

Date: 15.09.2020

I hereby declare that all information in this document has been obtained and presented in accordance with academic rules and ethical conduct. I also declare that, as required by these rules and conduct, I have fully cited and referenced all material and results that are not original to this work.

Name, Surname: Gamze Karataş

Signature :

ABSTRACT

SUPPRESSION OF TOOL TIP FRF IN MACHINE TOOL ASSEMBLIES BY COMPONENT MODE TUNING METHOD

Karataş, Gamze
Master of Science, Mechanical Engineering
Supervisor: Prof. Dr. H. Nevzat Özgüven
Co-Supervisor: Prof. Dr. Erhan Budak

September 2020, 89 pages

Chatter is a major problem in machining processes resulting in high amplitude vibrations and niose, poor surface finish, decreased life of the tool and mechanical components, thus limited productivity. Chatter stability of a machining process can be altered by modifying the tool tip frequency response function (FRF) of the machine tool assembly. Tool tip FRF of the machine tool assembly can be suppressed by creating tuned mass damper (TMD) effect among assembly components. In some milling applications, a holder extension can be added between the holder and the tool to increase the overall effective length for reaching far sections of a workpiece. In this thesis, an analytical design optimization procedure is presented to damp the most flexible mode of the spindle assembly by tuning the dimensions of the holder extension and the tool. As the first approach, the length of the holder extension is optimized to create modal interaction which suppresses the peak tool tip FRF. Then, both holder extension length and tool overhang length are optimized simultenaously to further increase the dynamic rigidity as a result of TMD effect. Additionally, the profile of the holder extension and the overhang length of the tool are tuned simulteneously to maximize the reduction in the peak tool tip FRF. Substantial improvements in tool tip FRF and chatter-free material removal rate (MRR) are

demonstrated through simulations. The results show that, there is a great potential for increased machining productivity caused by suppressed dominant mode of the assembly by tuning the dimensions of the holder extension length and the overhang tool length simultaneously creating maximized TMD effect.

Keywords: Chatter stability, Machine Tool Dynamics, FRF Modification, Tuned Mass Damper Effect, Design Optimization

ÖZ

TAKIM TEZGAHLARINDA TAKIM UCU FTF'SİNİN BİLEŞEN MODU EŞLEMESİ YÖNTEMİ İLE AZALTILMASI

Karataş, Gamze
Yüksek Lisans, Makina Mühendisliği
Tez Yöneticisi: H. Nevzat Özgüven
Ortak Tez Yöneticisi: Prof. Dr. Erhan Budak

Eylül 2020, 89 sayfa

Tırlama talaşlı imalat işlemlerinde yüksek genlikli titreşimlere ve sese, yüzey kalitesinin düşmesine, takımın ve mekanik bileşenlerin ömrünün azalmasına ve dolayısıyla verimliliğin azalmasına sebep olan büyük bir problemdir. Bir talaşlı imalat işleminin tırlama kararlılığı, takım ucu frekans tepki fonksiyonunun (FTF) modifikasyonu ile değiştirilebilir. Bir takım tezgahının takım ucu FTF'si bileşenler arasında ayarlı kütle sönümleyici (AKS) etkisi yaratılarak azaltılabilir. Bazı frezeleme işlemlerinde, takım tutucu ucundan uzağa ulaşılabilmesi için toplam efektif uzunluğu arttırmak amacıyla takım tutucu ile takım arasına takım tutucu uzatması eklenebilir. Bu tez çalışmasında, takım tutucu uzatması ve takımın boyutlarını ayarlayarak takım tezgahının en esnek modunu sönümlemek için analitik bir tasarım optimizasyonu yöntemi sunulmuştur. İlk yaklaşım olarak, takım tutucu uzatmasının boyu iş mili sisteminde tepe takım ucu FTF'sini baskılamak için modal etkileşim yaratılarak optimize edilmiştir. Ardından, hem takımın tutucu uzatmasının boyu hem de takımın boyu ayarlı kütle sönümleyici etkinin sonucu olarak dinamik rijitliği daha da arttırmak için eş-zamanlı olarak optimize edilmiştir. Ek olarak, takım tutucu uzatmasının profili ve takımın boyu tepe takım ucu FTF'sindeki azalmaları

maksimize etmek için eş-zamanlı olarak ayarlanmıştır. Takım ucu FTF'sindeki ve tırlamasız malzeme kaldırma hızındaki önemli iyileşmeler simülasyon sonuçları ile gösterilmiştir. Sonuçlar, takım tutucu uzatmasının boyutlarının ve takımın boyunun eş-zamanlı olarak optimize edilmesi ile maksimize edilmiş TMD etkisi yaratılacağını ve dolayısıyla sistemin baskın modunu baskılanması sebebiyle işleme verimliliğinin arttırılması için büyük bir potansiyel olduğunu göstermektedir.

Anahtar Kelimeler: Tırlama Kararlılığı, Tezgah Dinamiği, FRF Modifikasyonu, Ayarlı Kütle Sönümleyici Etki, Tasarım Optimizasyonu

To my family

ACKNOWLEDGMENTS

I would like to express my deepest gratitude to my supervisor Prof. Dr. H. Nevzat Özgüven and co-supervisor Prof. Dr. Erhan Budak for their excellent supervision, advice, criticism, encouragements and insight throughout all the stages of this research. Without their supervision, this thesis would not be complete.

I would like to thank Dr. Orkun Özşahin for his precious support throughout the thesis. I am very grateful for his suggestions and comments. I also would like to thank Prof. Dr. Ender Ciğeroğlu, who at first made me interested in mechanical vibrations and encouraged me take Mr. Özgüven's course.

I also would like to thank my assistant friends Cem Baykal and Sinan Şahin Candan. My sincere thanks to my beloved friends, Selin Özgül, Beril Kadıoğlu, Kamil Karaçuha and Stefan Hartl for being with me in every stage of my life. My special thanks to my precious students who encouraged me to be a better academic. Thanks to Kaveh in Sabancı in MRL for helping me in experiments.

I would like to give my deepest gratitude to my father Yener Karataş and my mother Ayşe Karataş for their never- ending support and endless love throughout my life. I would like to thank my brother Emre for his beautiful company.

TABLE OF CONTENTS

LIST OF TABLES

TABLES

LIST OF FIGURES

FIGURES

LIST OF ABBREVIATIONS

ABBREVIATIONS

FRF	: Frequency response function
TMD	: Tuned mass damper
MRR	: Material removal rate

LIST OF SYMBOLS

SYMBOLS

$b_{\lim}$	: Limiting chatter-free depth of cut
K_f	: Cutting force coefficient in chip thickness direction
m	: Average number of teeth in cut
$\mathrm{Re}\left[G(\omega)\right]$	: Real part of resulting FRF
$b_{\lim,abs}$	: Absolute stability limit
x	: Axial direction
$M(x,t)$	: Bending moment
$V(x,t)$	: Shear force
$y(x,t)$	: Displacement in the transverse (y) direction
$\psi(x,t)$	: Angle of rotation due to bending
$\beta(x,t)$	: Angle of rotation due to shear distortion
ρ	: Density
E	: Young Modules
G	: Shear Modules
k'	: Shear coefficient
A	: Cross section area
I	: Area moment of inertia of the cross section
L	: Beam element length
ν	: Poisson’s ratio

ω	: Excitation frequency
ω_r	: r-th elastic mode
t	: Time
$\overline{Y}(x)$	: Transverse displacement eigenfunction (not normalized)
$\overline{\Psi}(x)$	: Bending rotation eigenfunction (not normalized)
$\phi_r(x)$	: Normalized r-th transverse displacement eigenfunction
$\varphi_r(x)$	: Normalized r-th bending rotation eigenfunction
$\eta_r(t)$	: r-th mode time domain modal coordinate
H_{ij}	: Transverse displacement at coordinate i due to unit harmonic force excitation at point *j*
L_{ij}	: Transverse displacement at coordinate i due to unit harmonic moment excitation at point *j*
N_{ij}	: Bending rotation at coordinate i due to unit harmonic force excitation at point *j*
P_{ij}	: Bending rotation at coordinate i due to unit harmonic moment excitation at point *j*
γ	: Loss factor
$[A]$	: End point receptance matrix of system A
$[\alpha_A]$	: End point receptance matrix of system A (in rearranged form)
$[I]$	: Identity matrix
k_y	: Translational stiffness
k_θ	: Rotational stiffness
c_y	: Translational damping

c_θ : Rotational damping

ω_n : Natural frequency

ξ : Damping ratio

f : Frequency ratio

μ : Mass ratio

$\phi(x)$: Objective function

CHAPTER 1

INTRODUCTION

1.1 Literature Review

Chatter vibrations is one of the main problems in the machining industry. It results in unstable cutting, reduced material removal rate (MRR), poor surface finish and decreased life of tools and mechanical components. Therefore, it is one of the major obstacles which limit productivity and accuracy in machining processes. However, the recent advances in the machining industry, especially in aerospace, automotive and die/mold industries, demand more productive, precise, and stable machining processes. As a result, prediction and suppression of chatter have been, and will remain as, an essential interest of manufacturing research [1].

Chatter behavior of a machining process can be predicted by stability diagrams [2-5]. Stability diagrams provide stable (chatter-free) depth of cut and spindle speed pairs. A typical stability lobe diagram is shown in Figure 1.1.

The limiting chatter-free depth of cut in orthogonal cutting is given as [6]

$$b_{\lim} = \frac{-1}{2 \cdot K_f \cdot m \cdot \mathrm{Re}\left[G(\omega)\right]} \tag{1.1}$$

where K_f is the cutting force coefficient in chip thickness direction, m is the average number of teeth in cut, and $Re[G(\omega)]$ refers to the real part of the resulting FRF (in terms of receptance) at the cutting point. Absolute stability limit, $b_{lim,abs}$ is the maximum common stable depth of cut for all spindle speeds.

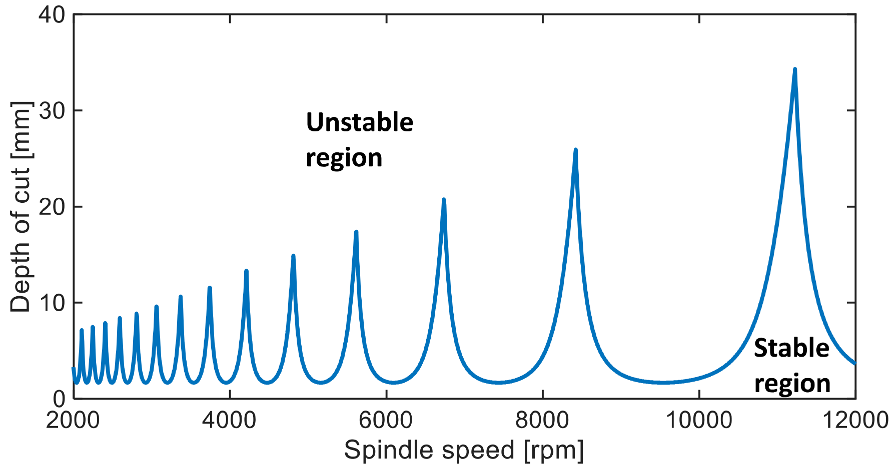

Figure 1.1 Stability diagram of a cutting process

As it can be seen from equation (1.1), the tool tip FRF of the machining assembly has great importance in the construction of stability lobe diagrams. In case of machining centers, the tool tip FRF is affected by the dynamics of all assembly components which are in general spindle, tool holder and tool. Clamping methods and interface dynamics between the assembly components have also predominant effect on the tool tip FRF.

Tool tip FRF is usually determined by experimental modal analysis which utilizes impact testing. In impact testing, a low mass accelerometer is placed to the tool tip and the assembly is excited by an instrumented impact hammer at the same point. However, measurements are unique to the assembly which is tested. Therefore, the measurements should be repeated for every spindle-holder-tool (THS) combination. Consequently, this approach is time consuming and impractical. These obstacles lead researchers to develop different techniques to obtain the tool tip FRF.

Schmitz et al. [7-10] developed a semi-analytical approach by using receptance coupling method to calculate the tool tip FRF. They determined the end point receptances of the tool analytically by using Euler-Bernoulli beam formulation. The dynamic information of the tool is then elastically coupled with the experimentally obtained holder tip dynamics of the spindle-holder subassembly considering holder-tool interface dynamics. The proposed method is a fast and accurate one to calculate the tool tip FRF especially for the cases where only the cutting tool is changed in the assembly provided that the holder-tool interface dynamics is accurately obtained.

In addition to the semi-analytical methods, Ertürk et al. [11-12] modeled the whole THS assembly analytically by using structural modification and receptance coupling methods. They modeled the assembly components with the Timoshenko beam theory, and their results are verified experimentally. They also showed that the Timoshenko beam formulation of machine tool components yield more accurate predictions compared to Euler-Bernoulli beam formulation in representing the dynamic behavior of the structure. Later, Özşahin et al. [13] predicted the tool tip FRF under operational conditions analytically by modeling the system components using rotating Timoshenko beam theory including gyroscopic effects.

Accurate identification of the contact parameters at the interfaces plays an important role in the accurate calculation of the tool tip FRF. In Schmitz's semi-analytical FRF prediction approach [7-10], the interfaces were modeled as translational and rotational springs and dampers located between the free end of the components. Later, Schmitz et al. [14] extended the model to have multiple coupling points in order to include the effect of contact interface of the tool within the holder. Additionally, they introduced the off-diagonal elements to the complex joint stiffness matrix. Ahmadi and Ahmadian [15] proposed to model the holder-tool interface as a distributed elastic layer to consider the variations in the stiffness due to changes in the tool overhang length. In [7-10] and [14-15], the experimentally obtained tool tip FRFs were fitted to the analytically determined tool tip FRFs by using non-linear least squares error minimization method in order to identify the contact parameters at the interfaces. Ertürk et al. [16] conducted an effect analysis on the THS assembly and showed that the first and second elastic mode of the assembly are controlled by the spindle-holder and the holder-tool interfaces, respectively. Based on this, Özşahin et al. [17] extracted the contact stiffness and damping values for the joint of interest. They performed an impact hammer test at the tool and the holder tip. Furthermore, they modeled the tool analytically by using Timoshenko beam formulation. Then, the contact parameters at the holder-tool interface were identified by using inverse receptance coupling approach with the corresponding experimentally obtained and analytically calculated FRFs. Similarly, the contact parameters at the spindle-holder interface were determined. Later, Özşahin et al. [18] implemented the artificial neural network theory to identify the contact dynamics at the interfaces and showed that the accuracy of the method was increased.

In order to avoid chatter and increase the stable zones in stability diagrams, one approach is to modify the dynamic behavior of the machine tool assembly. Chatter frequency is close to one of the most flexible mode(s), namely the critical mode(s) of the components involved in the machining system. Vibration control devices such as tuned mass dampers (TMDs) can be used to damp the critical mode of the assembly [1] yielding higher stability. TMD is a device attached to the main system in order to suppress the vibrations of the main system. Watts and Frahm [19-20] first applied the tuned mass dampers to reduce the rolling motion of ships. Ormondroyd and Den Hartog [21] developed the first theoretical bases of TMDs. Later, Den Hartog [22] found a closed form optimal solution for the stiffness and damping values of a TMD to have equal peaks in the response of the main system. Later, Randall et al. [23] obtained design curves for optimum TMD parameters based on minimax optimization criteria. They showed that minimization of the maximum amplitude of the displacement of the main system did not always bring equal resonance peaks, contrary to Den Hartog's [22] analytical work. TMDs bring an additional DOF to the system, and if their parameters are optimized, the critical mode of the assembly splits into two modes with smaller amplitudes increasing the stability limit of the cutting process. Tarng et al. [24] used a TMD to reduce the negative real part of the frequency response function of a cutting tool to improve the cutting stability in a turning operation. In [25], a boring bar is modeled as cantilevered uniform Euler-Bernoulli beam, and the optimum parameters of the TMD which improves the absolute stability limit are identified. Altıntaş et al. [26] improved the negative real part of the tool tip FRF by applying multiple TMDs to turning operations. In [26], it is shown that multiple TMDs need more accurate tuning of stiffness and natural frequency but more insensitive to the uncertainties in damping and input dynamic parameters of the system compered to single TMDs. The implementation of tuned mass dampers in milling processes has also been studied [27-28]. However, traditional approaches are not applicable to milling operations due to the high-speed rotation of the cutting tool. In [27], viscoelastic TMDs were applied to the workpiece to control the vibrations during a milling operation. Additionally, Yang et al. [28] designed a two-degree of freedom TMD having translation and rotation motion, and implemented it to the workpiece holding fixture to mitigate vibrations in a milling process. Similar to the results of [26], multiple degree of freedom TMDs are more robust in suppressing the critical mode of the assembly. Wang et al. [29-30] proposed the application of nonlinear TMDs with dry friction to enhance the chatter free behavior of machining operations. The performance of the nonlinear TMD is remarkable against the linear tuned mass dampers in avoiding chatter [29-30].

The critical mode of the assembly can be suppressed by changing the dynamics of the tool. Tool overhang tuning has been studied by many researchers. Tlusty et al. [31] adjusted the length of the tool to match its fundamental natural frequency with the integer multiple of the tooth passing frequency at the top speed of the spindle. The tool is modeled as cantilevered Euler-Bernoulli beam. They also showed that the MRR could be increased by increasing the length of the tool contrary to the intuition. Davies et al. [32] verified experimentally the numerical concept developed by Tlusty et al. [31]. Smith et al. [33] created a finite element model for spindle systems with different tools. They iteratively tuned the tool dimensions from a permissible range of tool lengths by using the method proposed by Tlusty et al. [31]. Later, Schmitz et al. [34] observed that the modal interaction among spindle assembly components could decrease the tool tip FRF resulting in improved stability limit. They matched the fundamental natural frequency of the cantilevered tool with one of the modes of the spindle-holder subassembly. As a result, the tool mode which is the critical one was split into two smaller modes similar to the dynamic absorber effect observed in tuned mass dampers. Similarly, Ertürk et al. [35] showed that it is possible to create dynamic absorber effect in the THS assembly by changing the dimensions of the components. The procedures in [34] and [35] are based on trial and error. Mohammedi et al. [36], on the other hand, developed a systematic and generalized procedure to tune the tool length to create modal interaction. The tool is modeled analytically as a free-free Timoshenko beam and they coupled the tool FRF with the experimentally obtained holder tip FRF by using the holder-tool interface dynamics. Then, the length of the tool is optimized to have equal peak in tool tip FRF similar to TMD optimization approach suggested by Den Hartog [22]. They also included the tool holder and spindle tail dimension tuning to the analysis as an alternative to the tool dimension tuning.

1.2 Objective

The aim of this thesis is a propose an analytical optimization procedure in machine tool structures to damp the most flexible mode of the assembly. This is achieved by increasing the dynamic rigidity of the structure by creating dynamic absorber effect within the subassemblies of the structure. In previous studies, tool overhang length or spindle tail dimension tuning and proper selection of tool holder to create modal interaction are proposed for that purpose. Nevertheless, in some applications it is not possible to shorten the length of the tool to create modal interaction or find a readily available holder that is suitable for tuning purposes. Moreover, spindle dimensions should be optimized in the design stage by the manufacturers. Therefore, a more practical solution is needed. In milling applications where a long tool is needed to reach far sections of a workpiece, an extension piece can be utilized between the holder and the tool to increase the overall effective length without increasing the cost since custom made tools are often needed for the same purpose. In this thesis, the dimensions of the holder extension are tuned to create dynamic interaction. Moreover, the dimensions of the tool and the holder extension are optimized simultaneously to maximize the dynamic rigidity of the spindle system. The improvements in the dynamic rigidity of the structure and chatter-free MRR are demonstrated by simulation results.

1.3 Layout of the Thesis

The outline of the thesis is as follows:

In Chapter 2, the basis of the tool tip FRF tuning methodology by proper design of component dimensions is presented. First, the dynamic modeling of the machine tool structure by receptance coupling and structural modification techniques with Timoshenko beam formulation is presented. Then, the basic theory of TMD is presented. A brief explanation of the optimization of tuned mass damper parameters is given. Finally, an analytical case study is conducted in which the tool length and spindle tail dimension are optimized in a THS assembly. Furthermore, a holder extension is employed between the same holder and the tool. Holder extension dimensions are optimized simultaneously with tool dimensions. The results of different tuning approaches are compared.

In Chapter 3, a sensitivity analysis in spindle-holder-holder extension-tool (TEHS) assembly is carried out. The effects of holder extension and tool dimensions on the tool tip FRF are investigated. Furthermore, the effect of holder-holder extension and holder extension-tool interface dynamics on the tool tip FRF are evaluated. The results of the analysis offer an insight into the dynamic behavior modification imposed by the changes in the design parameters of the holder extension and the tool.

In Chapter 4, the performances of different holder extension designs on tool tip FRF tuning are compared. Analytical case studies for these designs are conducted.

Finally, Chapter 5 provides the summary and conclusion of the thesis. Some suggestions are made for future work.

CHAPTER 2

REDUCTION OF TOOL TIP FRF BY COMPONENT MODE TUNING METHOD

2.1 Timoshenko Beam Theory

Dynamic characteristics of beam elements can be explained by basic beam theories in literature: Euler- Bernoulli beam, Rayleigh beam and Timoshenko beam theory. Euler-Bernoulli beam theory neglects the shear deformation and rotary inertia. This beam theory is accurate for beams with high slenderness ratio [37]. However, neglecting shear deformation and rotary inertia result in inaccurate estimation of, or overestimation of, natural frequencies for non-slender beams at higher frequencies. To overcome the problems of Euler-Bernoulli beam theory, Stephen Timoshenko [38-39] presented Timoshenko beam theory which accounts for the shear deformations as well as the rotary inertia. Timoshenko beam theory gives accurate results for any slenderness ratio. In this thesis, the Timoshenko beam theory is used to model the dynamic behavior of machine tool assembly.

Figure 2.1 shows a deformed Timoshenko beam element.

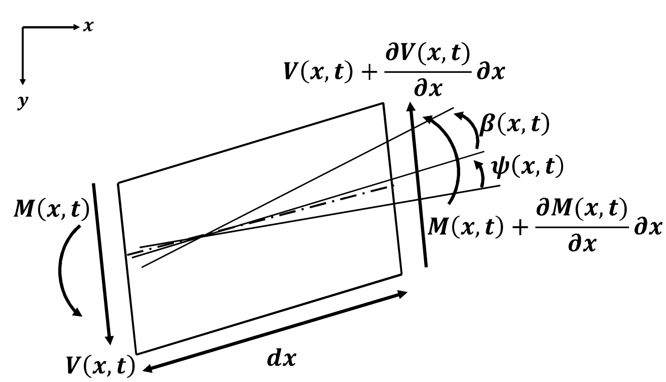

Figure 2.1 Deformed Timoshenko beam element

Here, $M(x,t)$ and $V(x,t)$ are the bending moment and shear force, respectively. The displacement in the transverse (y) direction is denoted by $y(x,t)$. $\psi(x,t)$ and $\beta(x,t)$ are the angle of rotation due to bending and shear distortion, respectively.

The governing uncoupled differential equation of motion when there is no external forcing can be written as follows [40]:

$$\frac{\partial^4 y(x,t)}{\partial x^4}-\left(\frac{\rho}{E}+\frac{\rho}{k'\cdot G}\right)\cdot\frac{\partial^4 y(x,t)}{\partial x^2\partial t^2}+\frac{\rho\cdot A}{E\cdot I}\cdot\frac{\partial^2 y(x,t)}{\partial t^2}+\frac{\rho^2}{k'\cdot E\cdot G}\cdot\frac{\partial^4 y(x,t)}{\partial t^4}=0 \tag{2.1}$$

$$\frac{\partial^4 \psi(x,t)}{\partial x^4}-\left(\frac{\rho}{E}+\frac{\rho}{k'\cdot G}\right)\cdot\frac{\partial^4 \psi(x,t)}{\partial x^2\partial t^2}+\frac{\rho\cdot A}{E\cdot I}\cdot\frac{\partial^2 \psi(x,t)}{\partial t^2}+\frac{\rho^2}{k'\cdot E\cdot G}\cdot\frac{\partial^4 \psi(x,t)}{\partial t^4}=0 \tag{2.2}$$

where ρ is density, E is young modules, G is shear modulus, k' is shear coefficient, A is cross section area and I is area moment of inertia of the cross section.

For a free-free Timoshenko beam element, the shear force and the bending moment are zero at the boundaries. Hence the boundary conditions of the uniform beam become

$$M(0,t)=E\cdot I\cdot\left.\frac{\partial\psi(x,t)}{\partial x}\right|_{x=0}=0 \tag{2.3}$$

$$M(L,t)=E\cdot I\cdot\left.\frac{\partial\psi(x,t)}{\partial x}\right|_{x=L}=0 \tag{2.4}$$

$$V(0,t)=k'\cdot A\cdot G\cdot\left.\left(\frac{\partial y(x,t)}{\partial x}-\psi(x,t)\right)\right|_{x=0}=0 \tag{2.5}$$

$$V(0,t)=k'\cdot A\cdot G\cdot\left.\left(\frac{\partial y(x,t)}{\partial x}-\psi(x,t)\right)\right|_{x=L}=0 \tag{2.6}$$

The eigenvalue problem of the uniform free-free Timoshenko beam is defined by equations (2.1) -(2.6). Assuming harmonic response in the time domain

$$y(x,t)=\overline{Y}(x)\cdot e^{i\omega t} \tag{2.7}$$

$$\psi(x,t) = \overline{\Psi}(x) \cdot e^{i\omega t} \tag{2.8}$$

The partial differential equations in (2.1) and (2.2) are converted into ordinary differential equations,

$$\frac{\partial^4 \overline{Y}(x)}{\partial x^4} + \omega^2 \cdot \left(\frac{\rho}{E} + \frac{\rho}{k' \cdot G} \right) \cdot \frac{\partial^2 \overline{Y}(x)}{\partial x^2} - \omega^2 \cdot \left(\frac{\rho \cdot A}{E \cdot I} - \omega^2 \frac{\rho^2}{k' \cdot E \cdot G} \right) \cdot \overline{Y}(x) = 0 \tag{2.9}$$

$$\frac{\partial^4 \overline{\Psi}(x)}{\partial x^4} + \omega^2 \cdot \left(\frac{\rho}{E} + \frac{\rho}{k' \cdot G} \right) \cdot \frac{\partial^2 \overline{\Psi}(x)}{\partial x^2} - \omega^2 \cdot \left(\frac{\rho \cdot A}{E \cdot I} - \omega^2 \frac{\rho^2}{k' \cdot E \cdot G} \right) \cdot \overline{\Psi}(x) = 0 \tag{2.10}$$

The characteristic equation of free-free Timoshenko beam can be written as [40]

$$\begin{vmatrix} D_{11} & D_{12} \\ D_{21} & D_{22} \end{vmatrix} = D_{11} \cdot D_{22} - D_{21} \cdot D_{12} = 0 \tag{2.11}$$

where

$$D_{11} = (\alpha - \lambda) \cdot (\cos\alpha - \cosh\beta) \tag{2.12}$$

$$D_{12} = (\lambda - \alpha) \cdot \sin\alpha + \frac{\lambda \cdot \alpha}{\beta \cdot \delta} \cdot (\beta - \delta) \cdot \sinh\beta \tag{2.13}$$

$$D_{21} = -\lambda \cdot \alpha \cdot \sin\alpha + \frac{\alpha - \lambda}{\delta - \beta} \cdot \sinh\beta \tag{2.14}$$

$$D_{22} = \lambda \cdot \alpha \cdot (\cosh\beta - \cos\alpha) \tag{2.15}$$

Here, α and β are the non-dimensional frequency numbers defined as

$$\alpha = \sqrt{\Omega + \varepsilon} \tag{2.16}$$

$$\beta = \sqrt{-\Omega + \varepsilon} \tag{2.17}$$

$$\Omega = \frac{b^2 \cdot (s^2 + R^2)}{2}, \varepsilon = b \cdot \sqrt{\frac{1}{4} \cdot b^2 \cdot (s^2 + R^2)^2 - (b^2 \cdot s^2 \cdot R^2 - 1)} \tag{2.18}$$

$$b^2=\frac{\rho\cdot A\cdot\omega^2\cdot L^4}{E\cdot I}, s^2=\frac{E\cdot I}{k^{'}\cdot A\cdot G\cdot L^2}, R^2=\frac{I}{A\cdot L^2} \tag{2.19}$$

By solving the characteristic equation given by (2.11), the natural frequency of the r-th elastic mode ω_r, and the corresponding non-dimensional frequency numbers α_r and β_r can be determined. The eigenfunction expressions for transverse displacement and bending rotation can be written as

$$\overline{Y_r}(x)=A_r\cdot\left[C_1\cdot\sin\left(\frac{\alpha_r}{L}\cdot x\right)+C_2\cdot\cos\left(\frac{\alpha_r}{L}\cdot x\right)\right.$$
$$\left.+C_3\cdot\sinh\left(\frac{\beta_r}{L}\cdot x\right)+C_4\cdot\cosh\left(\frac{\beta_r}{L}\cdot x\right)\right] \tag{2.20}$$

$$\overline{\Psi_r}(x)=\frac{A_r}{L}\cdot\left[\lambda_r\cdot\left(C_1\cdot\cos\left(\frac{\alpha_r}{L}\cdot x\right)-C_2\cdot\sin\left(\frac{\alpha_r}{L}\cdot x\right)\right)\right.$$
$$\left.+\delta_r\cdot\left(C_3\cdot\cosh\left(\frac{\beta_r}{L}\cdot x\right)+C_4\cdot\sinh\left(\frac{\beta_r}{L}\cdot x\right)\right)\right] \tag{2.21}$$

where

$$\lambda_r=\alpha_r-\frac{b^2\cdot s^2}{\alpha_r}, \delta_r=\beta_r+\frac{b^2\cdot s^2}{\beta_r} \tag{2.22}$$

$$C_1=L, C_2=-\frac{D_{11}}{D_{12}}, C_3=\frac{\alpha_r-\lambda_r}{\delta_r-\beta_r}, C_4=-\frac{\lambda_r\cdot\alpha_r}{\beta_r\cdot\delta_r}\cdot\frac{D_{11}}{D_{12}}\cdot C_1 \tag{2.23}$$
$$(r=1,2,3,...)$$

Here, A_r is the constant obtained by mass normalization of the eigenfunctions such that the following orthogonality condition is satisfied:

$$\int_0^L\left\{\overline{U}_s(x)\right\}^T\cdot\begin{bmatrix}\rho\cdot A & 0\\ 0 & \rho\cdot I\end{bmatrix}\cdot\left\{\overline{U}_r(x)\right\}\cdot dx=\begin{Bmatrix}1, s=r\\ 0, s\neq r\end{Bmatrix} \tag{2.24}$$

where

$$\left\{\overline{U}_r(x)\right\}=\begin{Bmatrix}\overline{Y}_r(x)\\ \overline{\Psi}_r(x)\end{Bmatrix} \tag{2.25}$$

Since free-free beam is considered, there are two rigid body modes. $y_0(x)$ and $\psi_0(x)$ represent the translational and rotational rigid body modes, respectively:

$$y_0(x) = \sqrt{\frac{1}{\rho \cdot A \cdot L}} \tag{2.26}$$

$$\psi_0(x) = \sqrt{\frac{12}{\rho \cdot A \cdot L^3}} \cdot \left(x - \frac{L}{2} \right) \tag{2.27}$$

By using the eigenfunction expansion theorem, the transverse displacement $y(x,t)$ and bending rotation $\psi(x,t)$ can be expressed as

$$y(x,t) = \sum_{0}^{\infty} \phi_r(x) \cdot \eta_r(t) \tag{2.28}$$

$$\psi(x,t) = \sum_{0}^{\infty} \varphi_r(x) \cdot \eta_r(t) \tag{2.29}$$

where $\phi_r(x)$ and $\varphi_r(x)$ are the mass normalized transverse displacement and bending rotation eigenfunctions, respectively. $\eta_r(t)$ is the time domain modal coordinate of the r-th mode.

The receptance matrix of free-free Timoshenko beam can be formulated as [11]

$$\left[B_{ij} \right] = \begin{bmatrix} H_{ij}^B & L_{ij}^B \\ N_{ij}^B & P_{ij}^B \end{bmatrix} \tag{2.30}$$

where H, L, N and P are the receptance functions defined in the following relationships:

$$H_{ij} = \frac{y_i}{F_j}; L_{ij} = \frac{y_i}{M_j}; N_{ij} = \frac{\psi_i}{F_j}; P_{ij} = \frac{\psi_i}{M_j} \tag{2.31}$$

where y_i and ψ_i are the transverse and rotational displacements at coordinate i, respectively. F_j and M_j are the applied force and bending moment at coordinate j, respectively.

The receptance functions of uniform free-free Timoshenko beam can be calculated as follows

$$H_{ij} = \sum_{0}^{\infty} \frac{\phi_r(x_i) \cdot \phi_r(x_j)}{(1 + i \cdot \gamma) \cdot \omega_r^2 - \omega^2} \tag{2.32}$$

$$L_{ij} = \sum_{0}^{\infty} \frac{\phi_r(x_i) \cdot \varphi_r(x_j)}{(1 + i \cdot \gamma) \cdot \omega_r^2 - \omega^2} \tag{2.33}$$

$$N_{ij} = \sum_{0}^{\infty} \frac{\varphi_r(x_i) \cdot \phi_r(x_j)}{(1 + i \cdot \gamma) \cdot \omega_r^2 - \omega^2} \tag{2.34}$$

$$P_{ij} = \sum_{0}^{\infty} \frac{\varphi_r(x_i) \cdot \varphi_r(x_j)}{(1 + i \cdot \gamma) \cdot \omega_r^2 - \omega^2} \tag{2.35}$$

where γ is the loss factor.

2.2 Mathematical Modeling of the Spindle System

In Section 2.1 receptance functions of uniform free-free Timoshenko beam are defined. However, the components of the spindle system consist of uniform segments with different diameters or sections with non-uniform profiles. Hence, the components of the spindle system cannot be modeled as a uniform single-segment beam. In this thesis, end point receptance matrices of the components are calculated by using rigid receptance coupling method. The bearing dynamics are added to the spindle by using the structural modification method suggested by Özgüven [41]. After end point receptance matrices of components are calculated, the dynamic information of the whole assembly is obtained by elastic receptance coupling of components considering the interface dynamics.

2.2.1 Receptance Coupling of the Component Segments

Multi-segment beams can be constructed by coupling of beams of different diameters and lengths with free end conditions. Consider Figure 2.2 in which two single segment beams with free end conditions A and B form two-segment beam C. First, consider the receptance matrix of beam A and B:

$$[A]=\begin{bmatrix}[A_{11}] & [A_{12}]\\ [A_{21}] & [A_{22}]\end{bmatrix} \tag{2.36}$$

$$[B]=\begin{bmatrix}[B_{11}] & [B_{12}]\\ [B_{21}] & [B_{22}]\end{bmatrix} \tag{2.37}$$

where

$$[A_{ij}]=\begin{bmatrix}H_{ij}^{A} & L_{ij}^{A}\\ N_{ij}^{A} & P_{ij}^{A}\end{bmatrix} \tag{2.38}$$

$$[B_{ij}]=\begin{bmatrix}H_{ij}^{B} & L_{ij}^{B}\\ N_{ij}^{B} & P_{ij}^{B}\end{bmatrix} \tag{2.39}$$

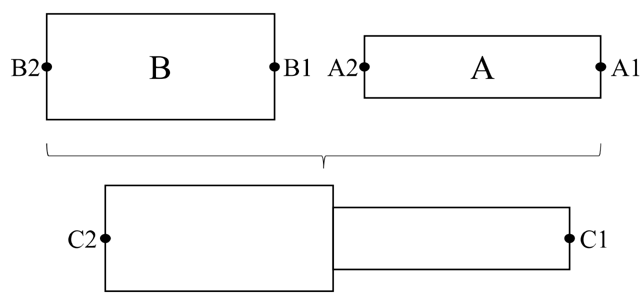

Figure 2.2 Rigid coupling of two beams

Then, the receptance matrix of multi-segment beam C can be obtained by using rigid receptance coupling through compatibility and continuity relations as [11]

$$[C]=\begin{bmatrix}[C_{11}] & [C_{12}]\\ [C_{21}] & [C_{22}]\end{bmatrix} \tag{2.40}$$

where

$$[C_{11}]=[A_{11}]-[A_{12}]\cdot\left[[A_{22}]+[B_{11}]\right]^{-1}\cdot[A_{21}] \tag{2.41}$$

$$[C_{12}]=[A_{12}]\cdot[[A_{22}]+[B_{11}]]^{-1}\cdot[B_{12}] \tag{2.42}$$

$$[C_{21}]=[B_{21}]\cdot[[A_{22}]+[B_{11}]]^{-1}\cdot[A_{21}] \tag{2.43}$$

$$[C_{22}]=[B_{22}]-[B_{21}]\cdot[[A_{22}]+[B_{11}]]^{-1}\cdot[B_{12}] \tag{2.44}$$

The end point receptances of an n-segment beam can be calculated by coupling of the segments with free end conditions using the chain coupling algorithm suggested by Ertürk et al. [11]. The same chain coupling algorithm can be utilized to calculate the end point receptance functions of beams with non-uniform profiles.

Consider the beam depicted in Figure 2.3. The end point receptance functions of the beam with a non-uniform profile can be obtained by discretizing the beam into n-segment beam.

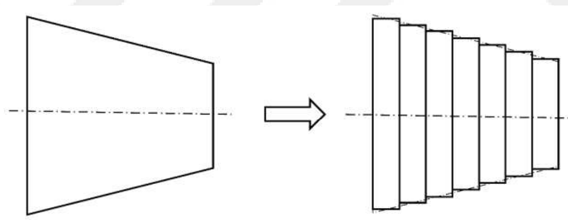

Figure 2.3 Beam with non-uniform profile

2.2.2 Addition of Bearing Dynamics with Matrix Inversion Method

As bearings support the spindle, the effect of bearing dynamics should be added where the bearing is located. The bearing dynamics can be added to the left end of a subcomponent of the spindle by using matrix inversion method [41]. Then, the remaining part of the spindle can be coupled to the modified system to construct the whole spindle by the receptance coupling method given in Section 2.2.1. The procedure is depicted in Figure 2.4.

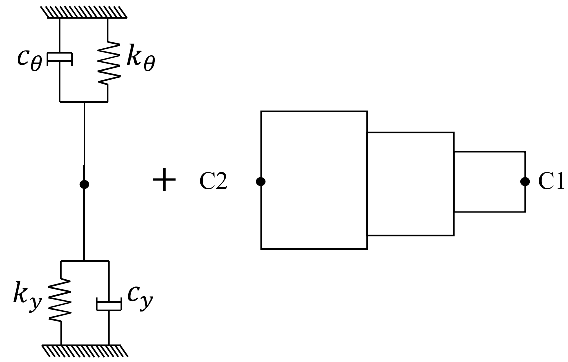

(a) Addition of bearing dynamics to the left end of a spindle subcomponent

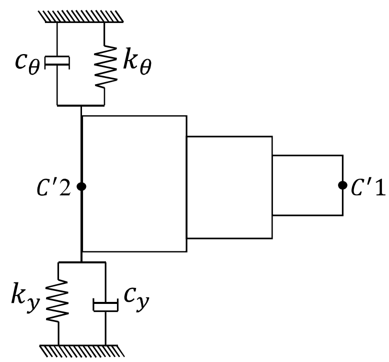

(b) Modified system

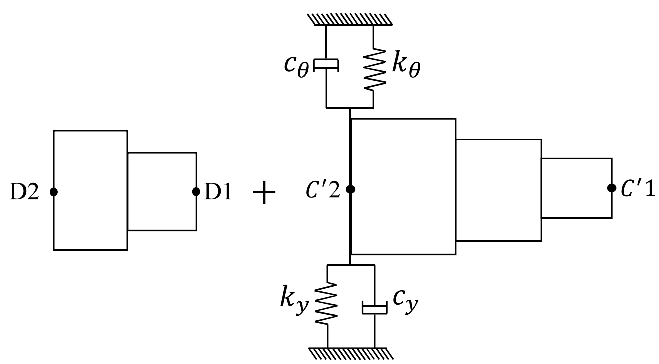

(c) Receptance coupling of modified system and the rest of the spindle

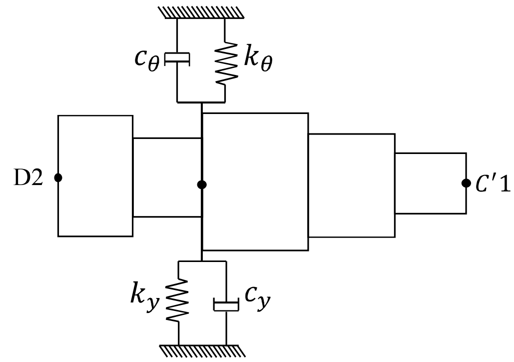

(d) Construction of the spindle with a bearing

Figure 2.4 The procedure to obtain dynamic information of the spindle with a bearing

The receptance matrix of the original system and the dynamic modification matrix of the bearings are needed to apply matrix inversion method. The receptance matrix of the unmodified system C can be formulated as explained in Section 2.2.1

$$[C]=\begin{bmatrix}\begin{bmatrix}H_{11}^{C} & L_{11}^{C}\\ N_{11}^{C} & P_{11}^{C}\end{bmatrix} & \begin{bmatrix}H_{12}^{C} & L_{12}^{C}\\ N_{12}^{C} & P_{12}^{C}\end{bmatrix}\\ \begin{bmatrix}H_{21}^{C} & L_{21}^{C}\\ N_{21}^{C} & P_{21}^{C}\end{bmatrix} & \begin{bmatrix}H_{22}^{C} & L_{22}^{C}\\ N_{22}^{C} & P_{22}^{C}\end{bmatrix}\end{bmatrix} \tag{2.45}$$

The receptance matrix given in equation (2.45) should be rearranged to apply matrix inversion method as follows

$$[\alpha_C]=\begin{bmatrix}\begin{bmatrix}\alpha_C{}^{11}\end{bmatrix} & \begin{bmatrix}\alpha_C{}^{12}\end{bmatrix}\\ \begin{bmatrix}\alpha_C{}^{21}\end{bmatrix} & \begin{bmatrix}\alpha_C{}^{22}\end{bmatrix}\end{bmatrix} \tag{2.46}$$

where

$$\begin{bmatrix}\alpha_C^{11}\end{bmatrix}=\begin{bmatrix}H_{11}^{C} & H_{12}^{C}\\ H_{21}^{C} & H_{22}^{C}\end{bmatrix} \tag{2.47}$$

$$\left[\alpha_C^{12}\right]=\begin{bmatrix} L_{11}^C & L_{12}^C \\ L_{21}^C & L_{22}^C \end{bmatrix} \tag{2.48}$$

$$\left[\alpha_C^{21}\right]=\begin{bmatrix} N_{11}^C & N_{12}^C \\ N_{21}^C & N_{22}^C \end{bmatrix} \tag{2.49}$$

$$\left[\alpha_C^{22}\right]=\begin{bmatrix} P_{11}^C & P_{12}^C \\ P_{21}^C & P_{22}^C \end{bmatrix} \tag{2.50}$$

The dynamic modification matrix of the bearings can be written as

$$\left[D\right]=\begin{bmatrix} \left[D^{11}\right] & [0] \\ [0] & [0] \end{bmatrix} \tag{2.51}$$

where

$$\left[D^{11}\right]=\begin{bmatrix} k_y+i\cdot\omega\cdot c_y & 0 \\ 0 & k_\theta+i\cdot\omega\cdot c_\theta \end{bmatrix} \tag{2.52}$$

The receptance matrix of the modified system C' in terms of partitioned matrices can be written [41] as

$$\left[\alpha_{C'}^{11}\right]=\left[\left[I\right]+\left[\alpha_C^{11}\right]\cdot\left[D^{11}\right]\right]^{-1}\cdot\left[\alpha_C^{11}\right] \tag{2.53}$$

$$\left[\alpha_{C'}^{12}\right]^T=\left[\alpha_{C'}^{21}\right]=\left[\alpha_C^{21}\right]\cdot\left[\left[I\right]-\left[D^{11}\right]\cdot\left[\alpha_{C'}^{11}\right]\right] \tag{2.54}$$

$$\left[\alpha_{C'}^{22}\right]=\left[\alpha_C^{22}\right]-\left[\alpha_C^{21}\right]\cdot\left[D^{11}\right]\cdot\left[\alpha_{C'}^{12}\right] \tag{2.55}$$

Here $[I]$ is the identity matrix.

Note that the receptance matrix $[C']$ should be rearranged to the form given in equation (2.45) to continue with the receptance coupling method.

2.2.3 Construction of Spindle-Holder-Tool (THS) Assembly by Elastic Receptance Coupling

A typical spindle-holder-tool (THS) assembly is depicted in Figure 2.5.

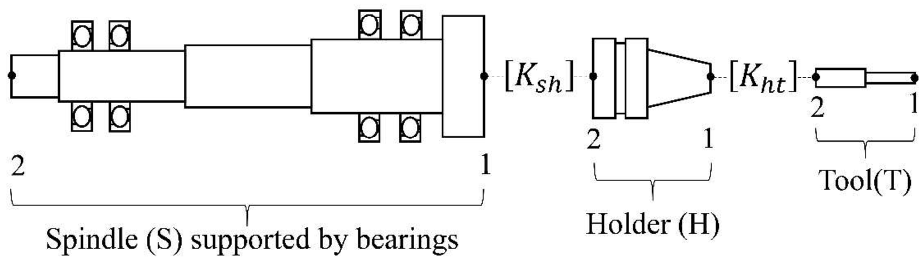

Figure 2.5 Spindle-holder-tool (THS) assembly

Once the end point receptance functions of each component are calculated, they can be coupled by considering the interface dynamics in order to construct the whole assembly.

In order to form spindle-holder (HS) subassembly by elastic receptance coupling, the end point receptance matrices of the spindle supported by bearing (S) and holder (H) should be calculated. The receptance matrix of the holder tip can be determined as [11]

$$[HS_{11}] = [H_{11}] - [H_{12}] \cdot \left[[H_{22}] + [K_{sh}]^{-1} + [S_{11}] \right]^{-1} \cdot [H_{21}] \tag{2.56}$$

Here $[K_{sh}]$ is the complex stiffness matrix representing the interface dynamics between the spindle and the holder [11]:

$$[K_{sh}] = \begin{bmatrix} k_y^{sh} + i \cdot \omega \cdot c_y^{sh} & 0 \\ 0 & k_\theta^{sh} + i \cdot \omega \cdot c_\theta^{sh} \end{bmatrix} \tag{2.57}$$

Having obtained the end point receptance matrix of spindle-holder subassembly at the holder tip, tool (T) should be coupled with the rest of the assembly to calculate the tool tip FRF matrix [11]:

$$[THS_{11}] = [T_{11}] - [T_{12}] \cdot \left[[T_{22}] + [K_{ht}]^{-1} + [HS_{11}] \right]^{-1} \cdot [T_{21}] \tag{2.58}$$

where $[K_{ht}]$ is the complex stiffness matrix representing the interface dynamics between the holder and the tool [11]:

$$[K_{ht}] = \begin{bmatrix} k_y^{ht} + i \cdot \omega \cdot c_y^{ht} & 0 \\ 0 & k_\theta^{ht} + i \cdot \omega \cdot c_\theta^{ht} \end{bmatrix} \tag{2.59}$$

Notice that the tool tip FRF matrix is in the following form

$$[THS_{11}] = \begin{bmatrix} H_{11}^{THS} & L_{11}^{THS} \\ N_{11}^{THS} & P_{11}^{THS} \end{bmatrix} \tag{2.60}$$

Also, note that, the tool tip FRF required to construct stability diagram is the receptance function related to the transverse displacement due to applied force, i.e. H_{11}^{THS}.

2.2.4 Construction of Spindle-Holder-Holder Extension-Tool (TEHS) Assembly by Elastic Receptance Coupling

A typical spindle-holder-holder extension-tool (TEHS) assembly is shown in Figure 2.6. An extension piece is employed between the holder and the tool.

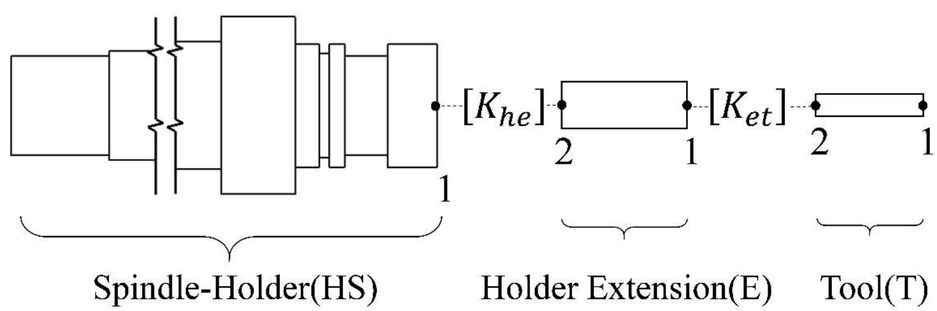

Figure 2.6 Spindle-holder-holder extension-tool (TEHS) assembly

Similarly, the dynamic response of the TEHS assembly can be predicted by receptance coupling and structural modification methods. The receptance matrix of the holder tip, $[HS_{11}]$, is already determined in Section 2.2.3. The receptance matrix of the holder extension tip can be calculated as follows:

$$[EHS_{11}] = [E_{11}] - [E_{12}] \cdot \left[[E_{22}] + [K_{he}]^{-1} + [HS_{11}] \right]^{-1} \cdot [E_{21}] \tag{2.61}$$

Here $[E_{11}]$, $[E_{12}]$ and $[E_{22}]$ are the direct and cross FRFs of the holder extension, respectively. $[K_{he}]$ is the interface dynamics between holder and holder extension:

$$[K_{he}] = \begin{bmatrix} k_y^{he} + i \cdot \omega \cdot c_y^{he} & 0 \\ 0 & k_\theta^{he} + i \cdot \omega \cdot c_\theta^{he} \end{bmatrix} \tag{2.62}$$

Next, the tool tip FRF matrix can be calculated as

$$[TEHS_{11}] = [T_{11}] - [T_{12}] \cdot \left[[T_{22}] + [K_{et}]^{-1} + [EHS_{11}] \right]^{-1} \cdot [T_{21}] \tag{2.63}$$

Similarly, $[K_{et}]$ is the interface dynamics between the holder extension and the tool:

$$[K_{et}] = \begin{bmatrix} k_y^{et} + i \cdot \omega \cdot c_y^{et} & 0 \\ 0 & k_\theta^{et} + i \cdot \omega \cdot c_\theta^{et} \end{bmatrix} \tag{2.64}$$

Again, the tool tip FRF required to construct stability diagram is the receptance function related to the transverse displacement due to the applied force, i.e. H_{11}^{TEHS}.

2.3 Theory of Tuned Mass Damper

Tuned mass damper (TMD) or tuned vibration absorber (TVA) is a device that is attached to a structure to suppress its vibrations. The vibration energy of the structure is transferred to the TMD when its natural frequency is tuned to a specific natural frequency of the structure. The theory of TMDs is first introduced by Frahm in 1909 and later, Den Hartog [22] established the theoretical bases of optimum tuning of TMDs for undamped main system in his book. The undamped TMD can be represented by a SDOF model as shown in Figure 2.7.

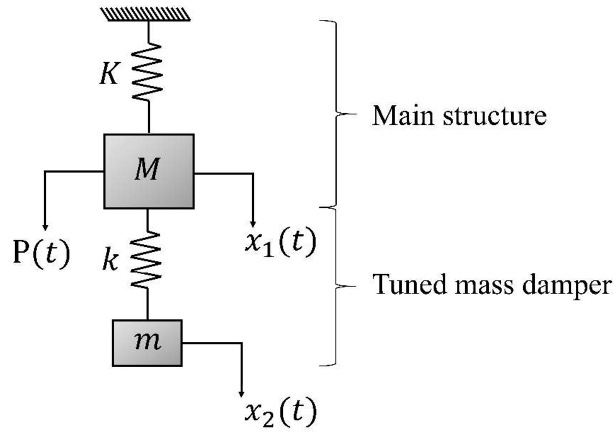

Figure 2.7 The undamped tuned mass damper

The main structure consists of a mass (M) and spring (K) with the harmonic force $P(t) = P_0 e^{i\omega t}$ acting on it. The mass and stiffness of the TMD are denoted by k and m, respectively. The equation of the motion of the 2-DOF system can be written as

$$M \cdot \ddot{x}_1 + (K + k) \cdot x_1 - k \cdot x_2 = P_0 \cdot e^{i \cdot \omega \cdot t} \tag{2.65}$$

$$m \cdot \ddot{x}_2 + k \cdot (x_2 - x_1) = 0 \tag{2.66}$$

The response of the system is of the form

$$x_1(t) = X_1 \cdot e^{i \cdot \omega \cdot t} \tag{2.67}$$

$$x_2(t) = X_2 \cdot e^{i \cdot \omega \cdot t} \tag{2.68}$$

Solving for X_1 and X_2 yields:

$$X_1 = \frac{P_0 \cdot (k - m \cdot \omega^2)}{(K + k - M \cdot \omega^2) \cdot (k - m \cdot \omega^2) - k^2} \tag{2.69}$$

$$X_2 = \frac{P_0 \cdot k}{(K + k - M \cdot \omega^2) \cdot (k - m \cdot \omega^2) - k^2} \tag{2.70}$$

As it can be seen from equation (2.69), the amplitude X_1 of the main structure becomes zero when the numerator $(k - m\omega^2)$ is equal to zero. When this equality is satisfied, the amplitude of X_2 becomes

$$X_2 = -\frac{P_0}{k} \tag{2.71}$$

Therefore, the force on the absorber is $-P_0 e^{i\omega t}$, which is actually equal and opposite to the excitation force. This phenomenon is described by Den Hartog [22] in his book as follows

'' The natural frequency $\sqrt{k/m}$ of the attached absorber is chosen to be equal to the frequency ω of the disturbing force. It will be shown that the main mass M does not vibrate at all, and that small system k, m vibrates in such a way that its spring force is at all instants equal and opposite to $P_0 e^{i\omega t}$. Thus, there is no net force acting on M and that mass does not vibrate. ''

In real life, damping always exists. The classical TMD system is formulated by Den Hartog [22]. The TMD with a damping element (c) attached to the main system is shown in Figure 2.8.

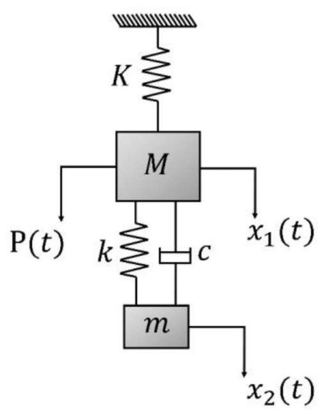

Figure 2.8 The classical damped tuned mass damper system

The equation of motion of the 2-DOF system becomes

$$M \cdot \ddot{x}_1 + K \cdot x_1 + k \cdot (x_1 - x_2) + c \cdot (\dot{x}_1 - \dot{x}_2) = P_0 \cdot e^{i \cdot \omega \cdot t} \tag{2.72}$$

$$m \cdot \ddot{x}_2 + k \cdot (x_2 - x_1) + c \cdot (\dot{x}_2 - \dot{x}_1) = 0 \tag{2.73}$$

For a classical TMD system, the amplitude of vibrations of the main system X_1 becomes

$$X_1 = \left| \frac{P_0 \cdot (k - m \cdot \omega^2 + i \cdot \omega \cdot c)}{(K + k - M \cdot \omega^2 + i \cdot \omega \cdot c) \cdot (k - m \cdot \omega^2 + i \cdot \omega \cdot c) - (k + i \cdot \omega \cdot c)^2} \right| \tag{2.74}$$

The objective of TMDs is to minimize the vibration amplitude of the main system given in equation (2.74). Den Hartog [22] suggested that the main system should have two equal resonance peaks for the most favorable response curve of the main system. The closed form analytical solution of the optimum parameters is

$$\xi_{opt} = \sqrt{\frac{3 \cdot \mu}{8 \cdot (1 + \mu)}}, f_{opt} = \frac{1}{1 + \mu} \tag{2.75}$$

where

$$\xi_{opt} = \frac{c}{2 \cdot \sqrt{k \cdot m}} \tag{2.76}$$

$$f_{opt} = \frac{\omega_a}{\omega_n}; \omega_a = \sqrt{\frac{k}{m}}; \omega_n = \sqrt{\frac{K}{M}} \tag{2.77}$$

$$\mu = \frac{m}{M} \tag{2.78}$$

The FRF of a main system with TMD is illustrated in Figure 2.9. The optimized TMD splits the main system response into two smaller modes with equal peaks around the main system’s resonance frequency.

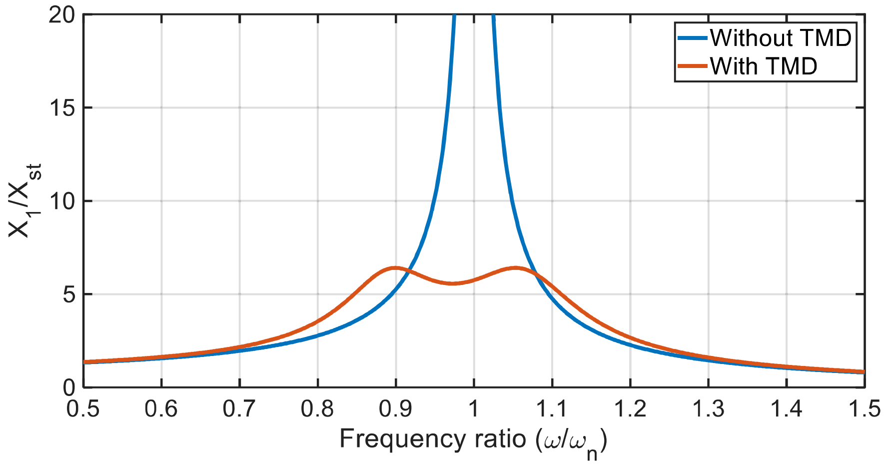

Figure 2.9 The amplitude of vibrations of the main system with and without TMD

2.4 Overview of the FRF Tuning Methodology

As discussed in the first chapter, the absolute depth of cut, $b_{lim,abs}$ of the machine tool assembly is inversely proportional to the negative real part of the oriented tool tip FRF [9]. Thus, $b_{lim,abs}$ can be increased by decreasing the amplitude of the tool tip FRF. Consider the THS assembly modeled as two substructures as shown in the Figure 2.10. In order to modify the dynamic behavior of the assembly, the effective modes in the holder tip FRF should be identified. These are the modes that are capable of being matched with the dominant mode of the assembly to create modal interactions among the substructures [36]. By optimizing the dimensions of the tool, the tool mode can be tuned to one of effective modes of the spindle-holder substructure. Similarly, by modifying the parameters of the spindle-holder substructure, one of the effective modes of the spindle-holder substructure can be shifted to the dominant mode of the cantilevered tool. As a result, the tool tip FRF splits into two smaller modes around the cantilevered tool mode similar to the absorber effect created by TMDs.

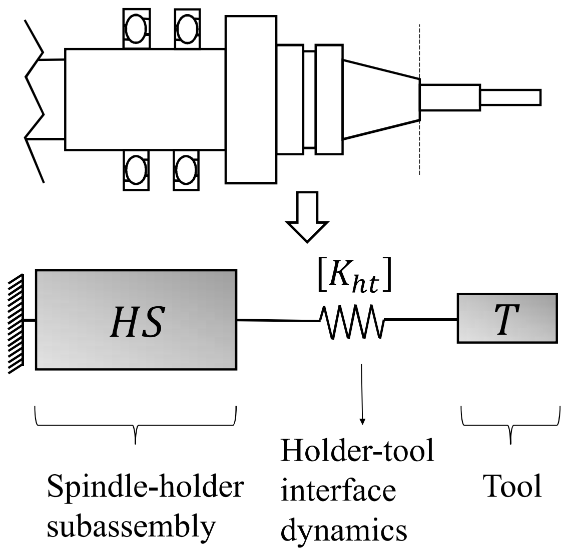

Figure 2.10 THS assembly modeled as two substructures

As discussed in Chapter 1, there are numerous optimization strategies for tuned mass dampers implemented to the machine tool assemblies. In this thesis, the objective is to find a suitable set of design parameters from permissible ranges which minimizes the maximum amplitude of tool tip FRF in the selected frequency range. The objective function $\phi(x)$ used in the optimization can be expressed as follows:

$$\phi(x) = \max\left(\left|H_{11}^{THS}\right|\right) \qquad (2.79)$$
$$x_{\min} \le x \le x_{\max}$$

Here, x represents the design parameters to be optimized. The optimization problem can be either one or a multi-variable case. It should be noted that, the objective function, $\Phi(x)$, can also be the maximum amplitude of the tool tip FRF of the TEHS assembly.

This is a discrete optimization problem since all the variables belong to a discrete set [42]. This is due to the fact that the design parameters such as holder extension length and tool overhang length can be changed at certain intervals. Moreover, the objective function is linear. Therefore, search based optimization formed in the permissible ranges would be sufficient to find the optimum design parameters which suppresses the peak tool tip FRF by creating TMD effect.

2.5 Modification of Tool Tip FRF by Component Mode Tuning: A Case Study

In this section, tool tip FRF of a typical THS assembly is predicted by the mathematical model given in Section 2.2. Then, the tool tip FRF is optimized by using the tuning methodology explained in Section 2.4. In the case studies, first, the tool overhang length is tuned to create modal interaction. Then, spindle tail dimensions are optimized instead of tool overhang length tuning. Secondly, an extension piece is added between the holder and tool in the same assembly. The tool tip FRF of the TEHS assembly is predicted by the same mathematical model. Furthermore, the length of the holder extension is optimized to create a dynamically stiffer system. Finally, the lengths of the tool and the holder extension are used as optimization parameters in the tuning methodology. The reductions in the tool tip FRF and improvements in the absolute stability limit, $b_{lim,abs}$, are also compared.

2.5.1 Case Study 1: Tool Overhang Length Tuning in THS Assembly

The dimensions of the components of the unmodified THS assembly used in the Case Study 1 are given in Table 2.1. The dynamic properties of the bearings and their locations are given in Table 2.2. The interface dynamics between the components are also given in Table 2.3.

Table 2.1 Dimensions of the assembly components for Case Study 1

(a) Spindle dimensions

Segment Number	1	2	3	4	5	6	7	8	9	10
Length[mm]	26	26	26	38	100	66	75	30	40	40
Outer Diameter[mm]	66	66	66	66	76	70	62	58	58	58
Inner Diameter[mm]	16	16	16	32	32	32	32	32	32	32

(b) Tool Holder dimensions

Segment Number	1	2	3
Length[mm]	22	19	24
Outer Diameter[mm]	72	60	70
Inner Diameter[mm]	0	16	16

(c) Tool dimensions

Segment Number	1	2
Length[mm]	24	26
Outer Diameter[mm]	6.5	8
Inner Diameter[mm]	0	0

Table 2.2 Dynamic properties and locations of the bearings for Case Study 1

(a) Dynamic properties of the bearings

	Translational Stiffness [N/m]	Translational Damping [N.s/m]
Front Bearings	7.5×10^5	100
Rear Bearings	2.5×10^6	100

(b) Location of the bearings

Bearing Number	1	2	3	4
Distance[mm]	26	78	387	427

Table 2.3 Interface dynamics between the components for Case Study 1

	Spindle-holder Interface	Holder-tool Interface
Translational Stiffness [N/m]	8×10^7	0.75×10^7
Translational Damping [N.s/m]	150	10
Rotational Stiffness [N.m/rad]	1.5×10^6	1.5×10^6
Rotational Damping [N.s.m/rad]	170	10

The material of all the components is steel with mass density of $\rho = 7800\ \mathrm{kg/m^3}$, Young modules $\mathrm{E} = 200$ GPa, Poisons ratio $\upsilon = 0.3$ with the material loss factor of $\gamma = 0.003$. The calculated tool tip FRF of the THS assembly with arbitrary tool overhang length (50 mm) is depicted in Figure 2.11. Blue dashed line shows cantilevered tool elastically coupled to the wall with interface dynamics $[\mathrm{K_{ht}}]$. Therefore, it can be concluded that the dominant mode of the assembly is controlled by the tool.

First of all, to tune the length of the tool, the effective modes in the holder tip FRF should be investigated. As it can be seen from Figure 2.12, there are effective modes at around 1010 Hz, 1930 Hz and 3625 Hz. The dominant mode of the assembly which is the tool mode is around 2250 Hz. The closest effective mode at 1930 Hz is chosen for suppression of the peak tool tip FRF.

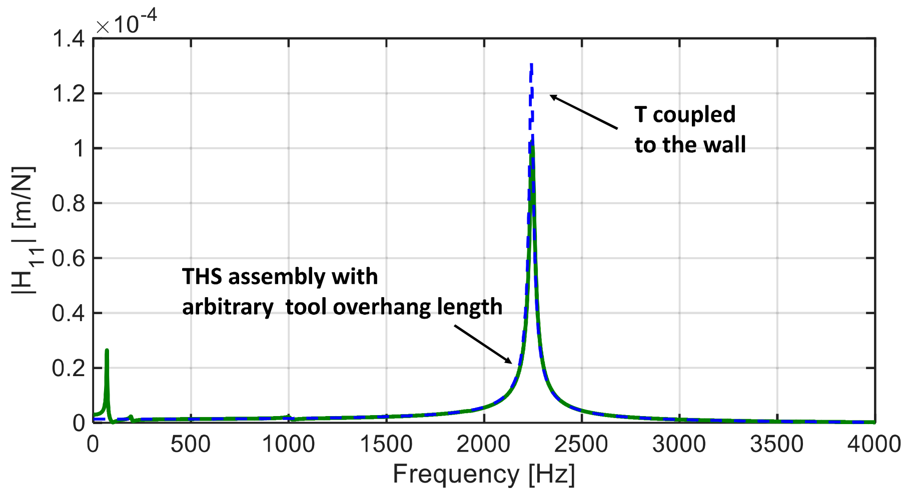

Figure 2.11 Tool tip FRF of the THS assembly with arbitrary tool overhang length (50 mm)

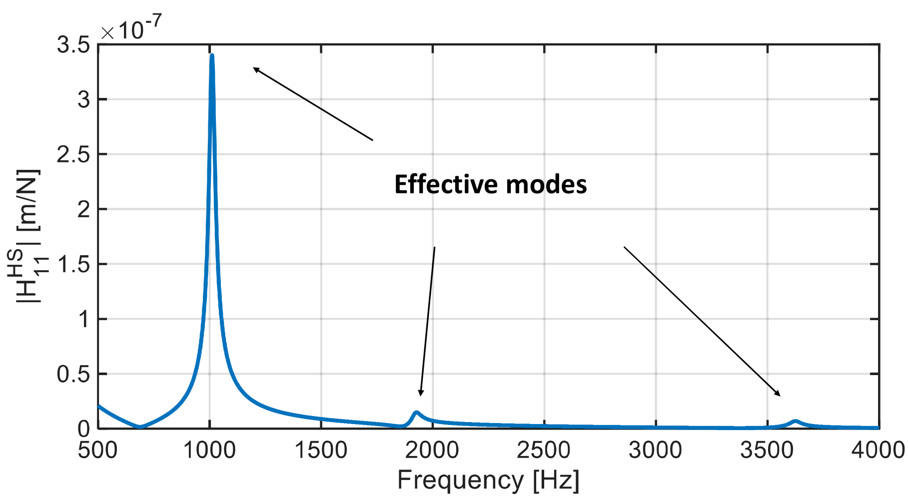

Figure 2.12 Effective modes in the holder tip FRF

The optimization problem is formulated as follows:

$$\phi(L_o) = \max\left(\left|H_{11}^{THS}\right|\right) \tag{2.80}$$
$$50mm \le L_O \le 60mm$$

where L_O is the tool overhang length. The variations in the maximum amplitude of the tool tip FRF with respect to tool overhang length is shown in Figure 2.13. Obviously increasing the tool overhang length increases the maximum amplitude of the tool tip FRF. However, there is a local minimum in the peak tool tip FRF when the overhang length of the tool is 55.5 mm.

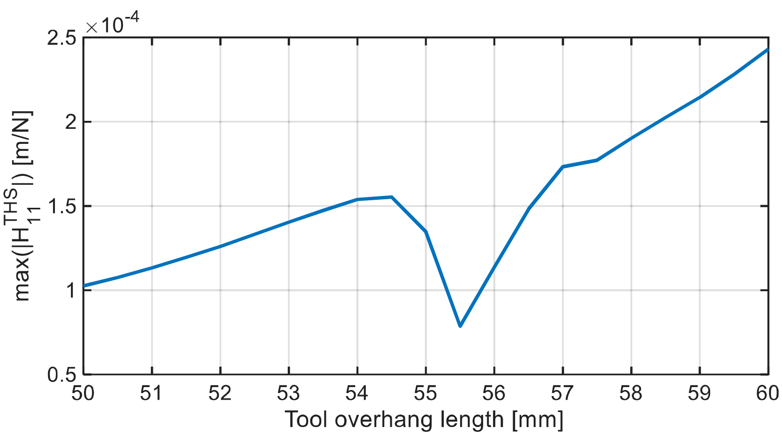

Figure 2.13 The effect of tool overhang length on the peak tool tip FRF

Figure 2.14 shows the modified tool tip FRF when the tool overhang length is 55.5 mm. As it can be seen, the fundamental frequency of the cantilevered tool is shifted to the chosen effective mode resulting in modal interaction between the substructures. Consequently, the dominant mode of the THS assembly splits into two smaller modes around the cantilevered tool mode. The peak tool tip FRF is decreased from 1×10^{-4} m/N to 0.75×10^{-4} m/N by tuning the tool overhang length as shown in Figure 2.15. Notice that, the peak tool tip FRF is decreased by increasing the overhang length of the tool, which is contrary to the common knowledge. The results show that, increasing the overhang length of the tool does not always decrease the dynamic rigidity of the assembly due to the absorber effect.

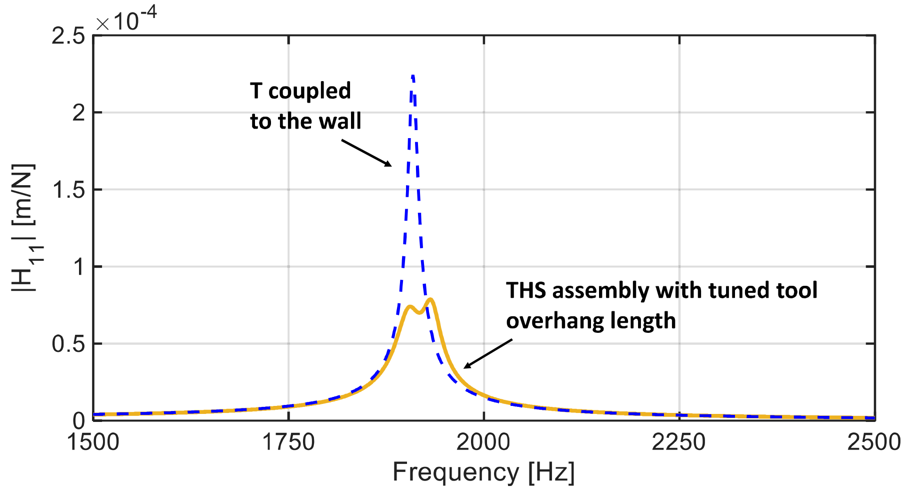

Figure 2.14 Tool tip FRF of the THS assembly with optimized tool overhang length (55.5 mm)

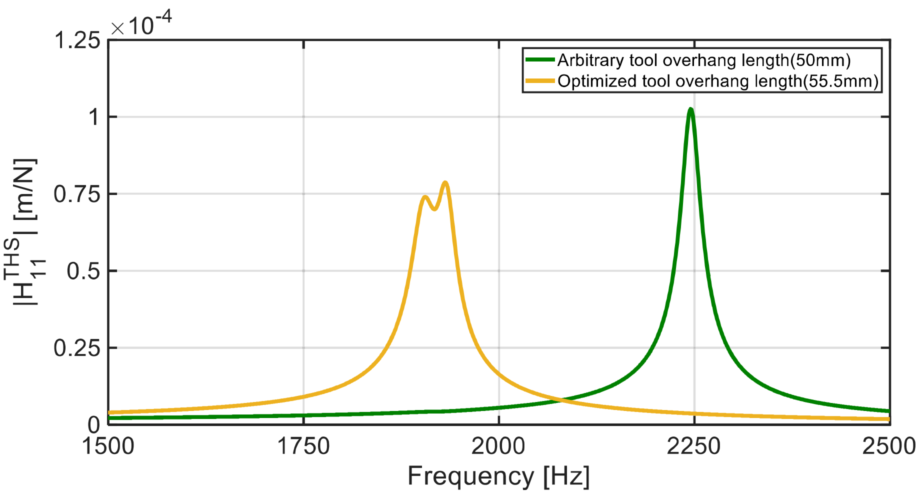

Figure 2.15 Comparison of tool tip FRFs of THS assembly with a tool having arbitrary overhang length (50 mm) and tuned overhang length (55.5 mm)

2.5.2 Case Study 2: Spindle Tail Dimension Tuning in THS Assembly

Mohammedi et al. [36] suggested that the tool tip FRF can be modulated by attaching an additional mass to the spindle tail. Consider the same THS assembly described in Case Study 1. As discussed in Section 2.5.1, there is an effective mode around 1930 Hz. Similar to the tool overhang length tuning, the dimension of the spindle can be optimized to shift the effective mode at 1930 Hz to the tool mode around 2250 Hz. Nevertheless, it is not possible to shift the effective mode at 1930 Hz to 2250 Hz by adjusting the spindle tail dimensions. Furthermore, it is not feasible to shift effective mode at 3625 Hz to the tool mode since the modes are too apart. Therefore, spindle tail dimension tuning is not applicable to the assembly described in Case Study 1. Instead, consider the THS assembly where another tool is clamped to the same spindle-holder subassembly in Case Study 1. Note that, interface dynamics between the tool and the holder changes when another tool is clamped. The tool dimensions and interface dynamics are given in Table 2.4.

Table 2.4 Dimensions of the tool and the interface dynamics for Case Study 2

(a) Tool Dimensions

Segment Number	1	2
Length[mm]	25	40
Outer Diameter[mm]	14	16
Inner Diameter[mm]	0	0

(b) Interface Dynamics

	Holder-tool Interface
Translational Stiffness [N/m]	1.5×10^{7}
Translational Damping [N.s/m]	10
Rotational Stiffness [N.m/rad]	1.5×10^{6}
Rotational Damping [N.s.m/rad]	10

Figure 2.16 illustrates the tool tip FRF of the THS assembly with the tool given in Table 2.4. The dominant mode of the assembly is shifted to the 1780 Hz. The effective modes are the same as the ones in the Case Study 1 since only the tool has changed.

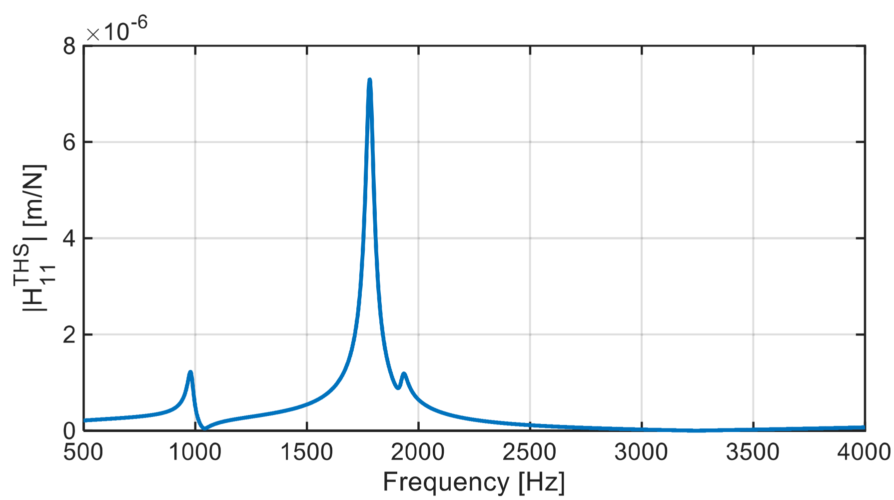

Figure 2.16 Tool tip FRF of the THS assembly without spindle tail

The optimization problem is formulated as follows:

$$\phi(L_t) = \max\left(\left|H_{11}^{THS}\right|\right) \tag{2.81}$$
$$10mm \le L_t \le 30mm$$

where L_t is the length of the spindle tail. The diameter of the spindle tail is assumed to be 58 mm. The length of the spindle tail which created dynamic absorber effect is found to be 16 mm. The tool tip FRF with tuned spindle tail is depicted in Figure 2.17. As seen from the Figure 2.17, the dominant mode of the assembly is diminished due to mode matching.

Notice that, the critical mode of the assembly remains unchanged when the spindle tail is tuned while it shifts to the chosen effective mode when the tool overhang length is tuned.

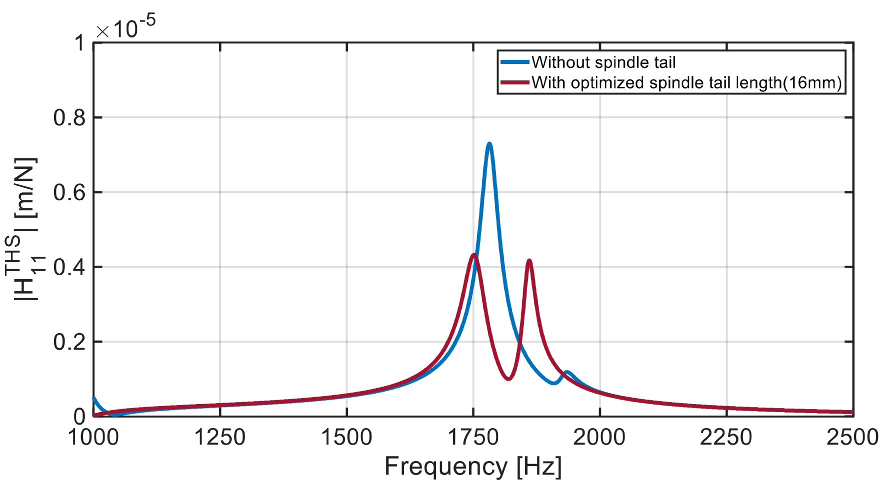

Figure 2.17 Comparison of tool tip FRFs of the THS assembly without spindle tail and with tuned spindle tail

2.5.3 Case Study 3: Holder Extension Length Tuning in TEHS Assembly

In this case study, the same spindle-holder combination described in Case Study 1 is used. The dimensions of the holder extension and the tool are given in Table 2.5. In the same table, the interface dynamics $[K_{he}]$ and $[K_{et}]$ are also given.

Table 2.5 Dimensions of the holder extension and interface dynamics for Case Study 3

(a) Holder extension dimensions

Segment Number	1
Length[mm]	40
Outer Diameter[mm]	16
Inner Diameter[mm]	0

(b) Tool dimensions

Segment Number	1	2
Length[mm]	24	26
Outer Diameter[mm]	6.5	8
Inner Diameter[mm]	0	0

(c) Interface dynamics

	Holder-holder extension Interface	Holder extension-tool Interface
Translational Stiffness [N/m]	2×10^7	0.75×10^7
Translational Damping [N.s/m]	150	10
Rotational Stiffness [N.m/rad]	1.5×10^6	1.5×10^6
Rotational Damping [N.s.m/rad]	170	10

Figure 2.18 shows the tool tip FRF of the unmodified TEHS assembly. Now, the dominant mode of the TEHS assembly is governed by the holder extension-tool subassembly. This is an expected result since the holder extension-tool subassembly

is the most flexible part of the whole system. The effective modes are the same as before since the parameters of the spindle-holder subassembly have not been changed.

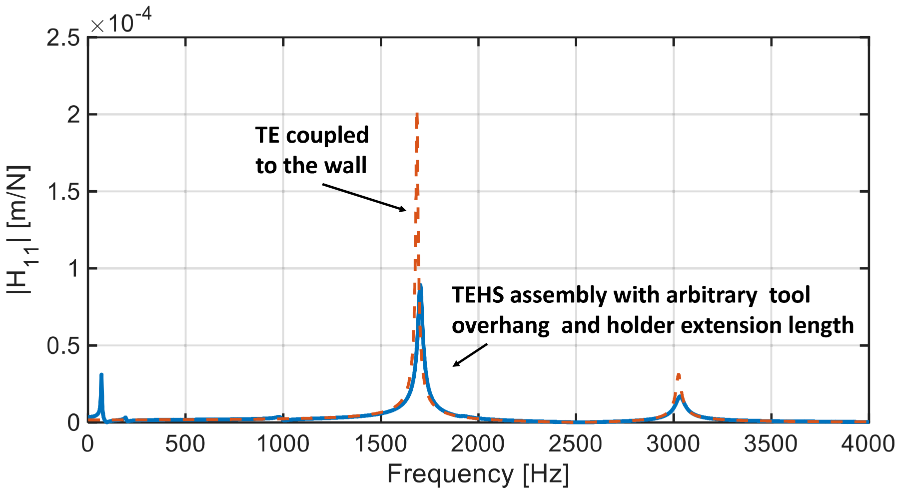

Figure 2.18 Tool tip FRF of the TEHS assembly with arbitrary holder extension length (40 mm) and arbitrary tool overhang length (50 mm)

The optimization problem is formulated as follows:

$$\phi(L_E) = \max\left(\left|H_{11}^{TEHS}\right|\right) \tag{2.82}$$
$$20mm \leq L_E \leq 50mm$$

where L_E is the length of the holder extension. The optimum holder extension length is searched between 20 mm and 50 mm. The maximum amplitude of tool tip FRF is minimized when the length of the holder extension is 24 mm. The tuned tool tip FRF of the TEHS assembly is given in Figure 2.19. By optimizing the length of the holder extension, the fundamental natural frequency of the cantilevered holder extension-tool subassembly is tuned to the effective mode at 1930 Hz. Consequently, the modal interaction between spindle-holder and holder extension-tool substructures results in dynamically stiffer system.

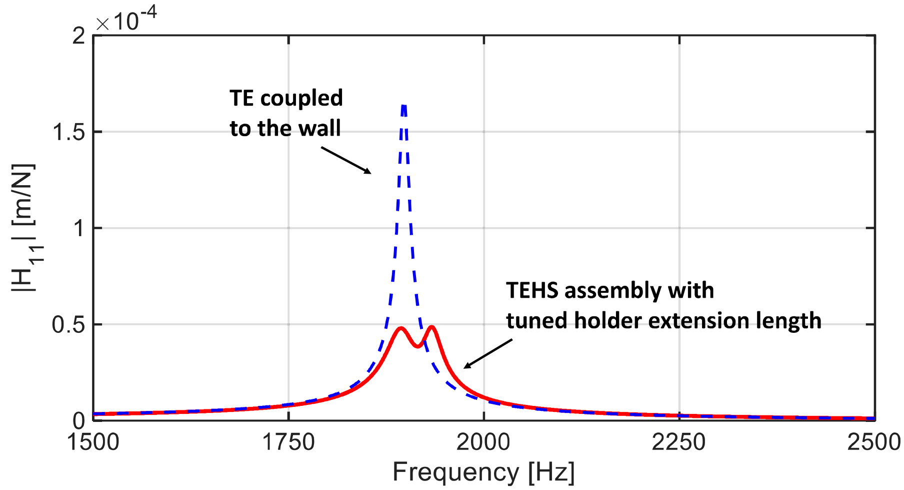

Figure 2.19 Tool tip FRF of the TEHS assembly with optimized holder extension length (24 mm) and arbitrary tool overhang length (50 mm)

2.5.4 Case Study 4: Holder Extension and Tool Overhang Length Tuning in TEHS Assembly

The same TEHS assembly in Section 2.5.3 is considered herein. The optimization problem is formulated as a multi-variable one in which both the holder extension length and tool overhang length are design parameters to be optimized.

The optimization problem becomes:

$$\begin{aligned} &\phi(L_E, L_O) = \max\left(\left|H_{11}^{TEHS}\right|\right) \\ &20mm \leq L_E \leq 50mm \\ &35mm \leq L_O \leq 55mm \end{aligned} \tag{2.83}$$

The maximum amplitude of tool tip FRF is plotted for different holder extension length and tool overhang length combinations in Figure 2.20. Dynamic absorber effect is created when the length of the holder extension and overhang length of the tool are 47 mm and 39 mm, respectively.

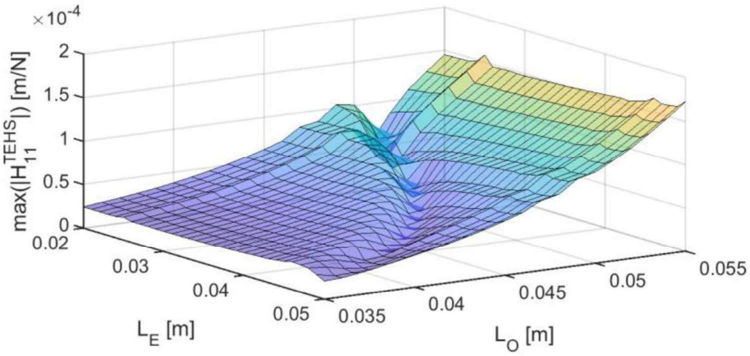

Figure 2.20 The effect of tool overhang length and holder extension length on the peak tool tip FRF

Figure 2.21 shows the tuned tool tip FRF with simultaneous optimization of holder extension length and tool overhang length. Again, the fundamental natural frequency of the cantilevered holder extension-tool subassembly is matched with the effective mode at 1930 Hz. Therefore, it can be concluded that, it is possible to tune the critical mode of the assembly with different combinations of the design parameters.

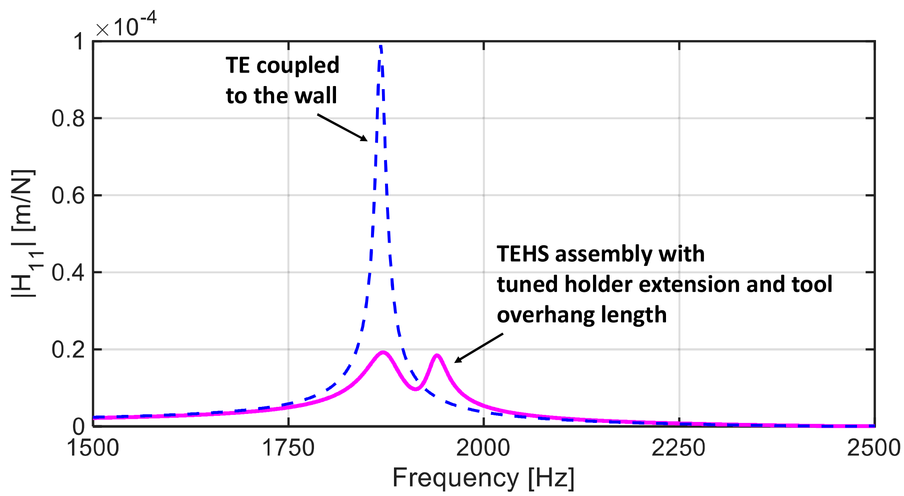

Figure 2.21 Tool tip FRF of the TEHS assembly with simultaneously optimized holder extension length (47 mm) and tool overhang length (39 mm)

Calculated tool tip FRFs of the TEHS assembly for Case Study 3 and Case Study 4 are compared in Figure 2.22. Notice that the overall effective length for the machining process is $74\ \mathrm{mm}$ in Case Study 3. On the other hand, it is $86\ \mathrm{mm}$ for Case Study 4. Obviously, decreasing the overall effective length from $90\ \mathrm{mm}$ to $74\ \mathrm{mm}$ increases the dynamic rigidity of the assembly. Nonetheless, with the multi-component dimension tuning which is obtained by simultaneous optimization of tool overhang length and holder extension length for Case Study 4 suppressed the dominant mode of the TEHS assembly from $0.9 \times 10^{-4}\ \mathrm{m/\ N}$ to $0.21 \times 10^{-4}\ \mathrm{m/\ N}$ while the effective length remains almost the same.

The yellow line shows the tool tip FRF of the TEHS assembly with separately optimized holder extension length ($24\ \mathrm{mm}$) and tool overhang length ($55.5\ \mathrm{mm}$) in Figure 2.22. The peak tool tip FRF of the TEHS assembly is increased to $1.6 \times 10^{-4}\ \mathrm{m/\ N}$ this time. This is an interesting result since the effective length is $89.5\ \mathrm{mm}$ while it is $90\ \mathrm{mm}$ for the unmodified TEHS assembly. This is due to the fact that increase in the tool overhang length increases the flexibility of the holder extension-tool subassembly resulting in decreased dynamic rigidity. Furthermore, as stated before, the peak tool tip FRF of the modified TEHS assembly in which the tool overhang length and holder extension length are optimized simultaneously is $0.21 \times 10^{-4}\ \mathrm{m/\ N}$. It can be concluded that, the optimization of the holder extension and the tool dimensions separately gives misleading results. The result shows that, the critical mode of the assembly is affected by the holder extension-tool subassembly as a whole. Therefore, the holder extension and the tool dimensions should be optimized simultaneously to create dynamic interaction between the spindle-holder subassembly and the holder extension-tool subassembly.

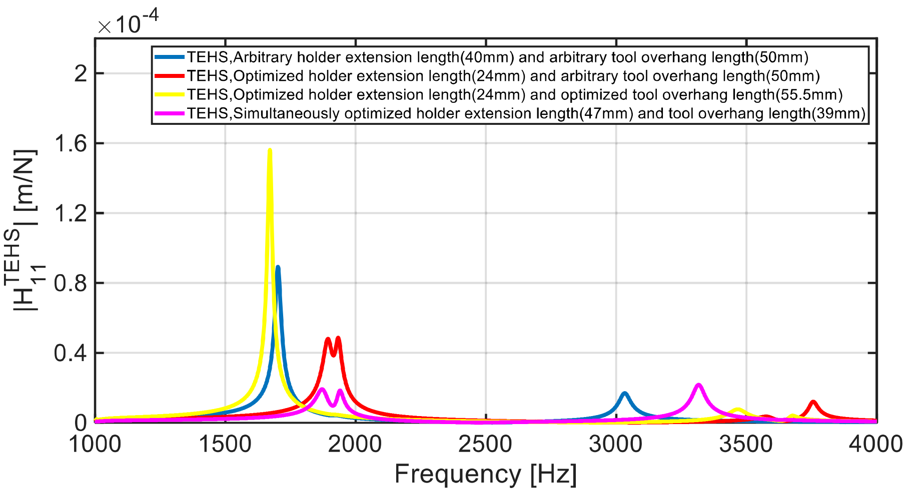

Figure 2.22 Comparison of tool tip FRFs of TEHS assemblies with optimized component dimensions

2.5.5 Comparison of Reductions in the Tool Tip FRF and Chatter Simulations

As stated before, tool overhang length tuning in THS assemblies has been studied by many researchers. However, to the best of author's knowledge, the topology optimization of the holder extension piece by taking advantage of the dynamic absorber effect has not been studied before. In this section, the effectiveness of the holder extension dimension tuning in contrast to tool overhang length tuning is compared.

In Figure 2.23, the green line shows the tool tip FRF of the THS assembly with arbitrary tool overhang length (50 mm). The red line illustrates that, the tool tip FRF of the spindle system can be reduced more than two times when a tuned holder extension is utilized between the holder and the tool in the same assembly. Additionally, more than five times reduction in the tool tip FRF is obtained with the multi-component dimension tuning of the holder extension length and the tool overhang length simultaneously. It is also worth to note that, the overall effective length is increased from 50 mm to 86 mm while there is a remarkable reduction in the peak tool tip FRF. On the other hand, the peak tool tip FRF of the modified TEHS assembly in which holder extension and tool overhang lengths are optimized separately is higher than the peak tool tip FRF of the THS assembly with arbitrary tool overhang length. This observation shows the importance of the simultaneous optimization of the holder extension and the tool dimensions.

It has been observed that there are several effective modes in the holder tip FRF that can be chosen for suppression of the peak tool tip FRF. The effective mode at 3625 Hz could also be used for damping purposes. In this case, the tuned overhang length of the THS assembly would be found to be 34 mm. The peak tool tip FRF of the modified THS assembly will be 1.39×10^{-5} m/N if the overhang length is chosen to be 34 mm, as shown in Figure 2.23. In general, shortening the overhang length of the tool without addition of a holder extension would give better results in the suppression of the peak tool tip FRF for the spindle-holder combination analyzed. However, then the overall effective length is to be decreased considerably which should be avoided in some machining operations.

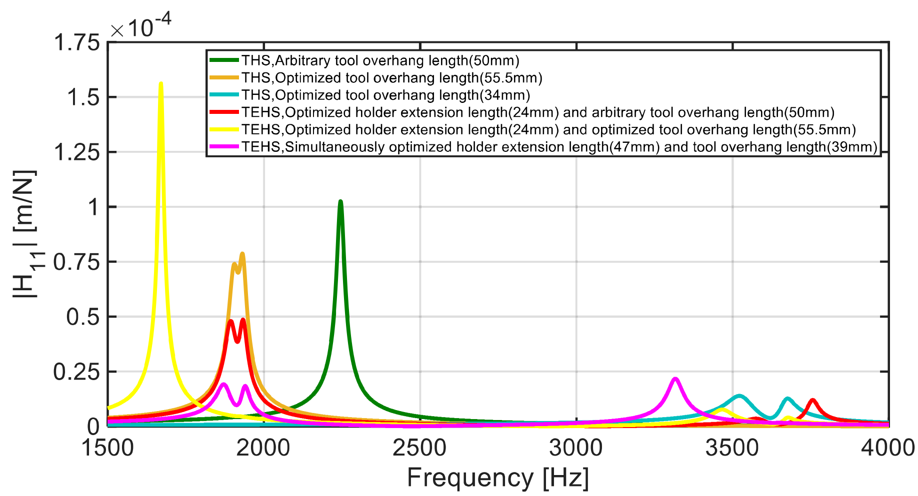

Figure 2.23 Tool tip FRFs with optimized component dimensions

The corresponding stability lobe diagrams predicted using the tool tip FRFs with optimized component dimensions are given in Figure 2.24. The corresponding absolute stability limits are also given in Table 2.6. As it can be seen, there is a noticeable improvement in the stable area in the existence of the tuned extension piece while the overall effective length is increased. Chatter-free depth of cut and in turn MRR of a cutting process can be further improved by tuning the dimensions of the tool and the holder extension simultaneously. Therefore, an optimized holder extension-tool subassembly can enhance the productivity in high-speed applications, especially in aerospace, where usage of long and slender cutting tools is inevitable.

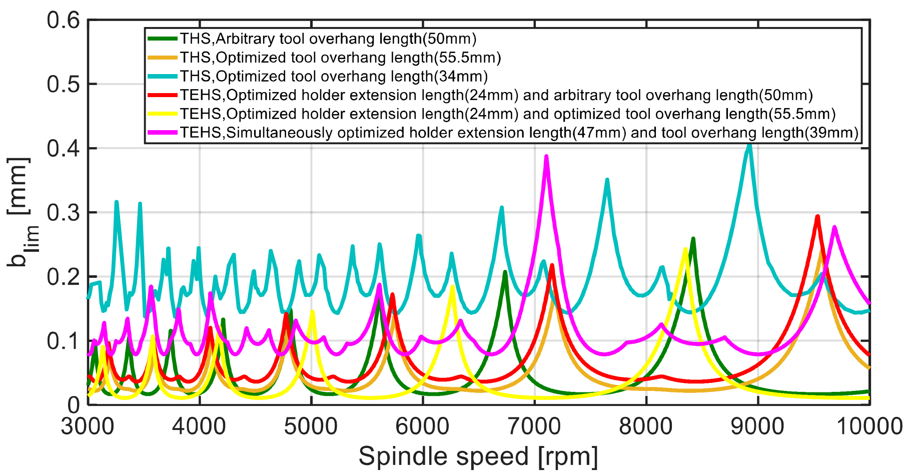

Figure 2.24 Stability lobe diagrams predicted using the tool tip FRFs with optimized component dimensions

Table 2.6 Comparison of absolute stability limits

	$b_{lim,abs}$ [mm]	Percent increase in $b_{lim,abs}$
THS, $L_O = 50$ mm	0.0167	-
THS, $L_O = 55.5$ mm	0.0220	31.7 %
THS, $L_O = 34$ mm	0.1447	766.47%
TEHS, $L_O = 50$ mm, $L_E = 24$ mm	0.0362	116.8 %
TEHS, $L_O = 39$ mm, $L_E = 47$ mm	0.0788	371.9%
TEHS, $L_O = 55.5$ mm, $L_E = 24$ mm	0.0109	-34.7%

CHAPTER 3

EFFECT ANALYSIS IN SPINDLE-HOLDER-HOLDER EXTENSION-TOOL (TEHS) ASSEMBLIES

In this chapter, the effects of design parameters of the holder extension-tool subassembly on tool tip FRF are investigated in order to understand dimension tuning capacity in TEHS assemblies. As discussed in Chapter 2, by tuning the most flexible mode of the assembly to the effective mode, the peak tool tip FRF can be suppressed due to dynamic interaction similar to the TMD systems. Therefore, the design parameters of the most flexible part play an important role in FRF tuning methodology.

3.1 Investigation of the Contribution of the Components to the Dominant Mode of the Assembly

Consider the TEHS assembly given in Section 2.5.3. The tool tip FRF of the assembly is shown in Figure 3.1. To investigate the most flexible part of the assembly, the FRFs of the holder extension-tool subassembly and only the tool are also plotted when they are coupled to the wall with the corresponding interface dynamics. The natural frequencies of the assembly obtained using the given analytical method are given in Table 3.1.

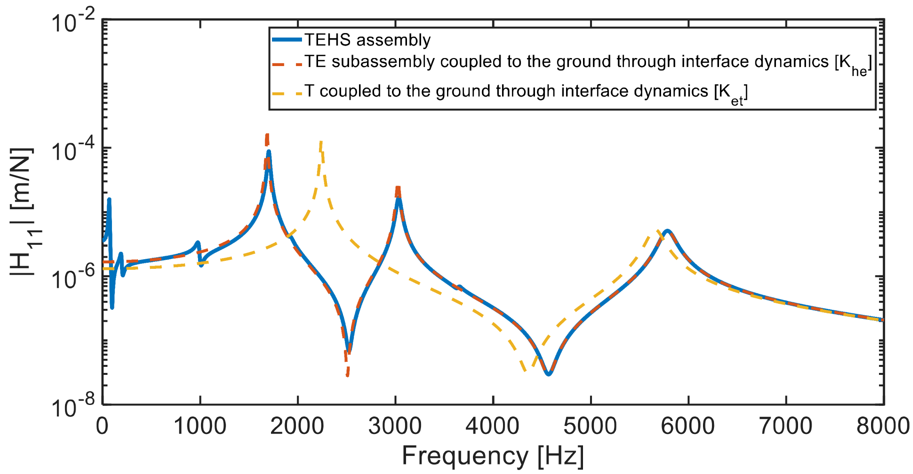

Figure 3.1 Tool tip FRF of the TEHS assembly

Table 3.1 Natural frequencies of the assembly

Mode Number	1	2	3	4	5	6	7	8
[Hz]	70	189	977	1703	1920	3034	3654	5785

The first two modes of the TEHS assembly are the rigid body modes as shown by Ertürk et al. [35]. As it can be seen from the Figure 3.1, the dominant mode of the assembly is the second elastic mode around 1700 Hz. The cantilevered holder extension-tool subassembly has modes around 1700 Hz, 3000 Hz and 5800 Hz which contribute to the second, fourth and sixth elastic modes of the whole assembly. Therefore, the most flexible mode results from the holder extension-tool substructure. Also note that, the cantilevered tool has a mode at 5800 Hz. As a result, it can be concluded that, the sixth elastic mode of the assembly is sensitive to the changes in tool parameters.

3.2 Sensitivity Analysis

3.2.1 Effect of Holder-Holder Extension Interface Dynamics

The sensitivity of tool tip FRF in changes in the interface dynamics at the holder-holder extension connection is studied here. As shown by Ertürk et al. [35], the rotational stiffness has negligable effect on the resulting tool tip FRF. Furthermore, damping in the interfaces does not affect the natural frequencies of the assembly. As a result, only the translational stiffness at the interfaces is taken into account in the effect analysis.

The same TEHS assembly in Section 3.1 is considered herein. The translational stiffness between the holder and the holder extension is first halved then doubled as shown in Figure 3.2. It is observed that, the variations in the translational stiffness strongly controls the fourth elastic mode of the assembly which is dominated by the second mode of the cantilevered holder extension-tool subassembly. Nevertheless, the dominant mode of the assembly is the second elastic mode, i.e. the first mode of the cantilevered holder extension-tool subassembly. As it can be seen from the Figure 3.2, the second elastic mode of the TEHS assembly is not affected that much.

At first, one could propose that, identification of the translational stiffness at the holder-holder extension interface is not crucial in analytical design optimization of the holder extension-tool subassembly by creating dynamic absorber effect. This proposal is investigated on the modified assembly described in Section 2.5.4. In Section 2.5.4, the simultaneously optimized holder extension and tool overhang length are found to be $47\ \mathrm{mm}$ and $39\ \mathrm{mm}$, respectively, when the translational stiffness at the holder-holder extension connection is $2 \times 10^{-7}\ \mathrm{N/m}$. Figure 3.3 shows the effect of translational stiffness at the holder extension-tool interface on the tool tip FRF of the modified assembly with $47\ \mathrm{mm}$ long holder extension and $39\ \mathrm{mm}$ tool overhang. The variations in the translational stiffness between the holder and the holder extension completely change the dynamic behavior of the second and the fourth elastic mode of the modified TEHS assembly. This is due to the fact that, this time, the first and the second modes of the cantilevered holder extension-tool subassembly are sensitive to the changes in translational stiffness at the holder-holder extension interface. Therefore, the interface dynamics between the holder and the holder extension should be identified properly. Additionally, when the translational stiffness between the holder and the holder extension is 1×10^{-7} N/m, the dominant mode of the TEHS assembly shifts to the forth elastic mode. As a result, in some applications, the second mode of the cantilevered holder extension-tool subassembly has to be tuned with the effective mode to suppress the vibrations of the tool tip.

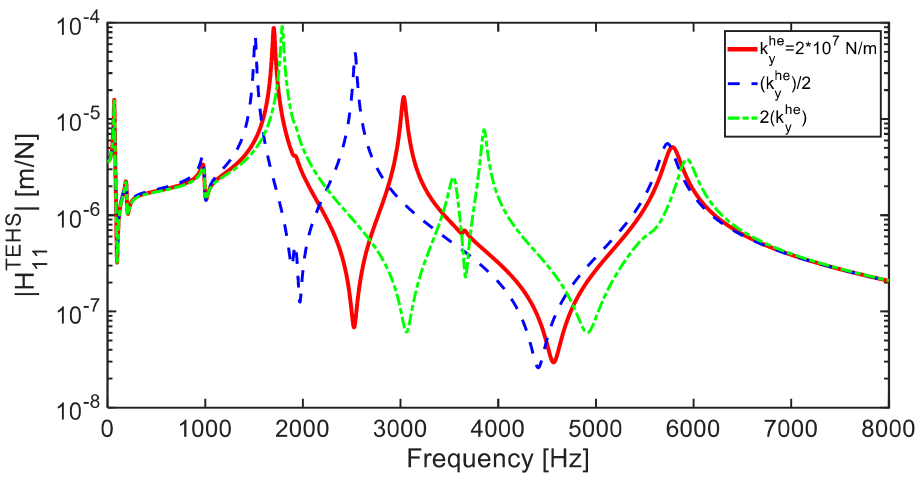

Figure 3.2 The effect of translational stiffness at the holder-holder extension interface on the tool tip FRF of the unmodified assembly

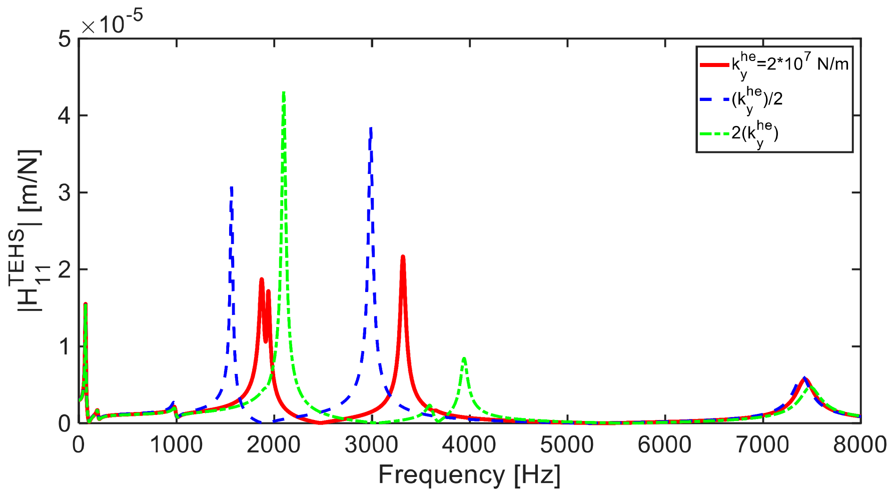

Figure 3.3 The effect of translational stiffness at the holder-holder extension interface on the tool tip FRF of the modified assembly

3.2.2 Effect of Holder Extension-Tool Interface Dynamics

Figure 3.4 shows the effect of translational stiffness between the holder extension and the tool in the same system. It is observed that, the translational stiffness at the holder extension-tool interface strongly controls the sixth elastic mode of the assembly analyzed which is controlled by the third mode of the cantilevered holder extension-tool subassembly. This stems from the fact that, cantilevered tool with the holder extension-tool interface dynamics dominates the third mode of the cantilevered holder extension-tool subassembly as described in Section 3.1. On the other hand, translational stiffness at the holder extension-tool interface has negligible effect on the dominant mode of the TEHS assembly analyzed, i.e. second elastic mode. Similarly, the variations in the tool tip FRFs of the modified assembly due to changes in the translational stiffness at the holder extension-tool interface is given in Figure 3.5. Similar to the results of Section 3.2.1, the interface dynamics between the holder extension and the tool should be identified properly in order to modify the dominant mode of the TEHS assemblies by creating dynamic interaction among the assembly components.

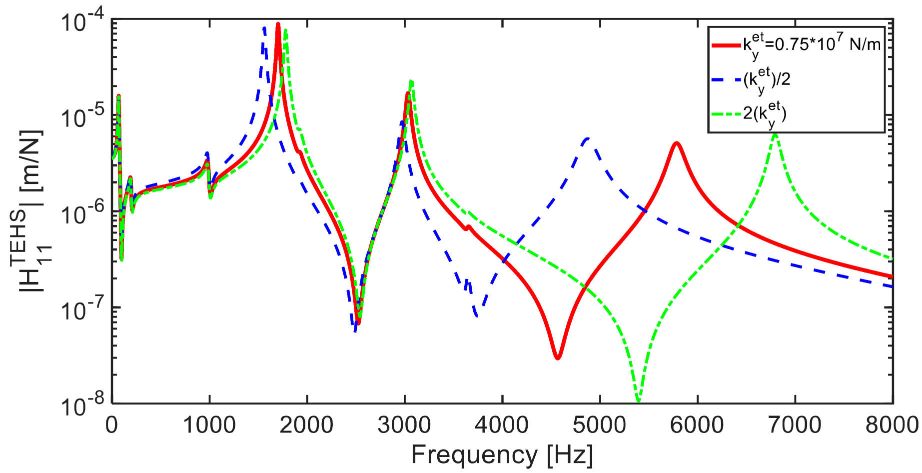

Figure 3.4 The effect of translational stiffness at the holder extension-tool interface on the tool tip FRF of the unmodified assembly

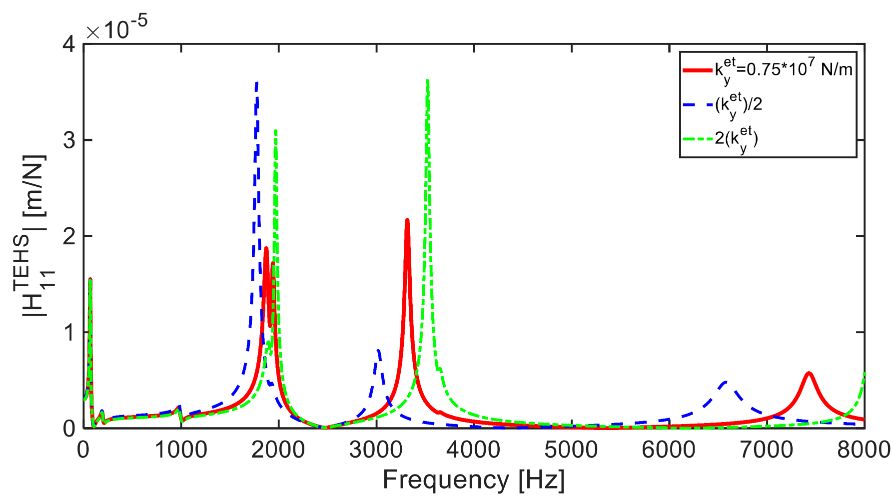

Figure 3.5 The effect of translational stiffness at the holder extension-tool interface on the tool tip FRF of the modified assembly

3.2.3 Effect of Holder Extension Geometry

3.2.3.1 Effect of Length of the Holder Extension

The length (40 mm) of the holder extension of the assembly described in Section 3.1 is first decreased to 20 mm and then increased to 60 mm in order to see the effect of the holder extension length on the resulting tool tip FRF. As it can be seen from Figure 3.6, the second, the fourth and the sixth elastic modes of the assembly shift due to changes in the length of the holder extension. As shown in Section 3.2.1, the most flexible mode of the TEHS assembly can be either governed by the first or the second mode of the cantilevered holder extension-tool subassembly. As a result, since the most flexible mode of the TEHS assembly can be modified due to the changes in the length of the holder extension, it is useful to tune the length of the holder extension to create dynamic absorber effect.

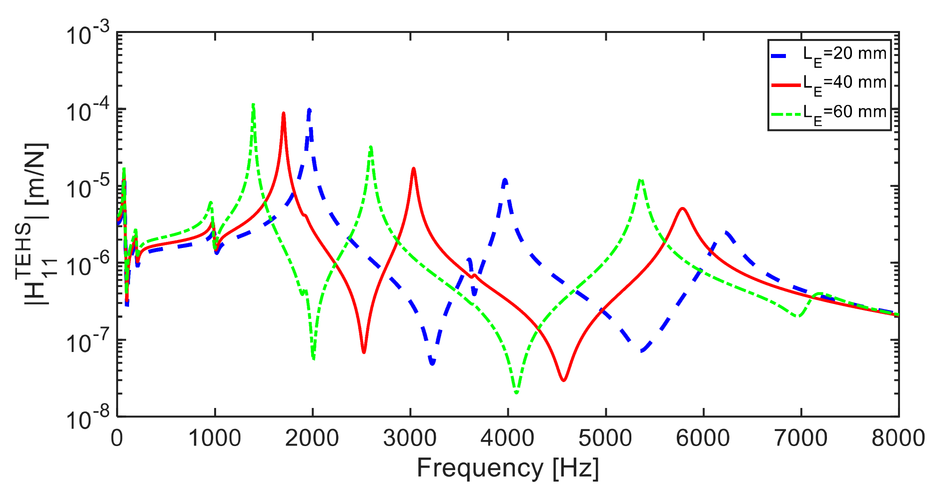

Figure 3.6 The effect of the holder extension length on tool tip FRF

3.2.3.2 Effect of Diameter of the Holder Extension

The variations in the tool tip FRF due to change in the diameter of the holder extension is shown in Figure 3.7. As it can be seen from Figure 3.7, as the diameter of the holder extension is increased from 16 mm to 27 mm, the frequency of the dominant mode of the TEHS assembly increases. This is due the fact that dynamic rigidity of the holder extension-tool subassembly increases as the slenderness ratio (L/D) of the holder extension decreases from $50:27$ to $50:40$. Conversely, the dominant mode of the assembly slightly shifts to lower values as the diameter of the holder extension is increased from 27 mm to 40 mm. This arises from the fact that as the holder extension becomes a non-slender structure, holder extension acts as a mass. Thefore, the most flexible part of the TEHS assembly becomes the tool.

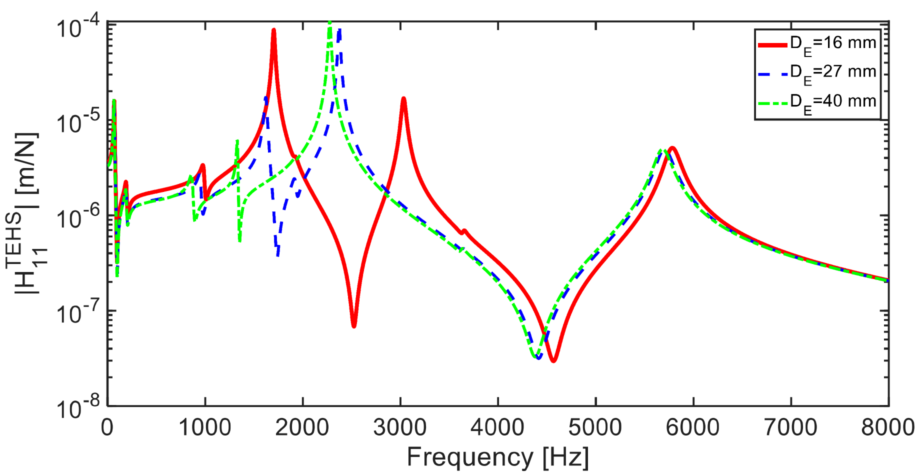

Figure 3.7 The effect of diameter of the holder extension on tool tip FRF

3.2.3.3 Effect of Profile of the Holder Extension

It is possible to design holder extensions with different profiles. In this section, the effect of the taper ratio of the holder extension on the resulting tool tip FRF is investigated. The taper ratio of the holder extension is defined as the diameter ratio (D_2/D_1) as shown in Figure 3.8.

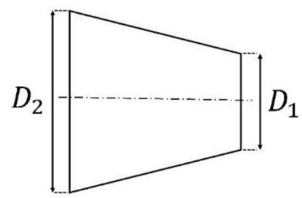

Figure 3.8 Tapered beam

The taper ratio of the holder extension described in Section 3.1. is first increased from 1 to 1.25 then to 1.5 while the diameter D_1 of the holder extension is maintained as 16 mm. The resulting tool tip FRFs are depicted in Figure 3.9. It is observed that the taper ratio of the holder extension particularly controls the fourth elastic mode of the TEHS assembly analyzed. Therefore, it can be concluded that for the assembly analyzed, the dynamic behavior of the second mode of the cantilevered holder extension-tool subassembly can be modified by changing the profile of the holder extension. On the other hand, the increase in the taper ratio slightly shifts the dominant mode of the assembly, i.e. the second elastic mode of the TEHS assembly analyzed, to lower values due the mass addition effect.

The sensitivity of the tool tip FRF of the modified assembly to the changes in the taper ratio of the holder extension is shown in Figure 3.10. Again, the second elastic mode of the assembly is controlled by the profile of the holder extension. Therefore, it can be concluded that, depending on the dimensions of the holder extension-tool subassembly components, the dominant mode of the assembly can be altered by tuning the profile of the holder extension.

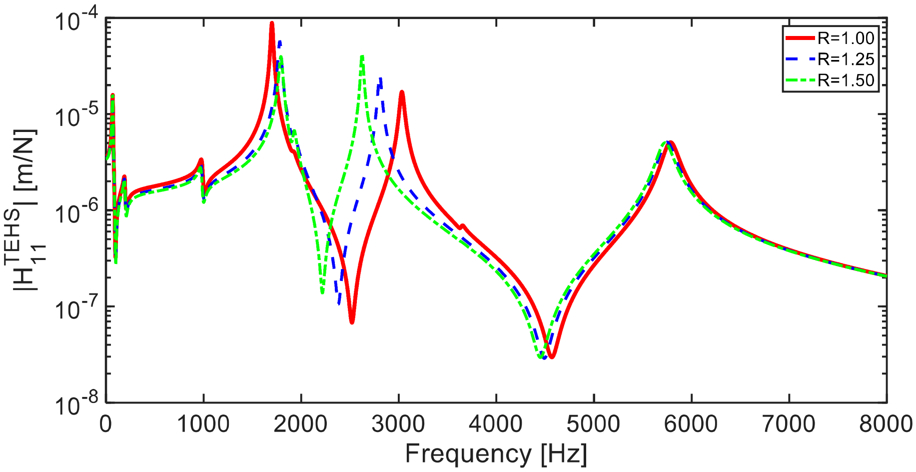

Figure 3.9 The effect of taper ratio of the holder extension on tool tip FRF of the unmodified assembly

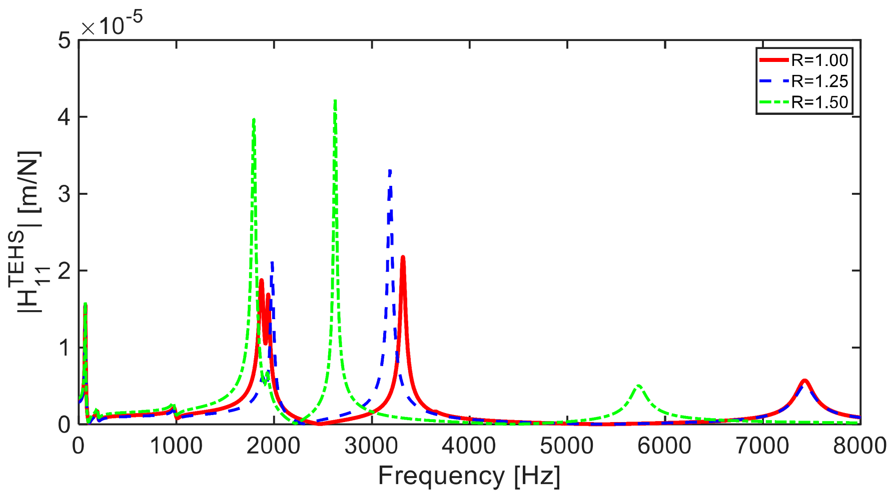

Figure 3.10 The effect of taper ratio of the holder extension on tool tip FRF of the modified assembly

3.2.4 Effect of Tool Geometry

Investigation of the effects of the diameter and the overhang length of the tool on the resulting tool tip FRF of the same TEHS assembly described in Section 3.1 is conducted herein. The diameter of the tool is first increased from 8 mm to 10 mm then to 12 mm while keeping the overhang length of the tool 50 mm. As it can be seen from the Figure 3.11, the dominant mode of the assembly can be altered by changing the diameter of the tool. Similarly, the overhang length of the tool is decreased by 10 mm while the diameter is 8 mm assuming interface dynamics remain constant as depicted in Figure 3.12. It can be concluded that the dominant mode of the assembly can be easily modified by adjusting the overhang length of the tool in TEHS assemblies.

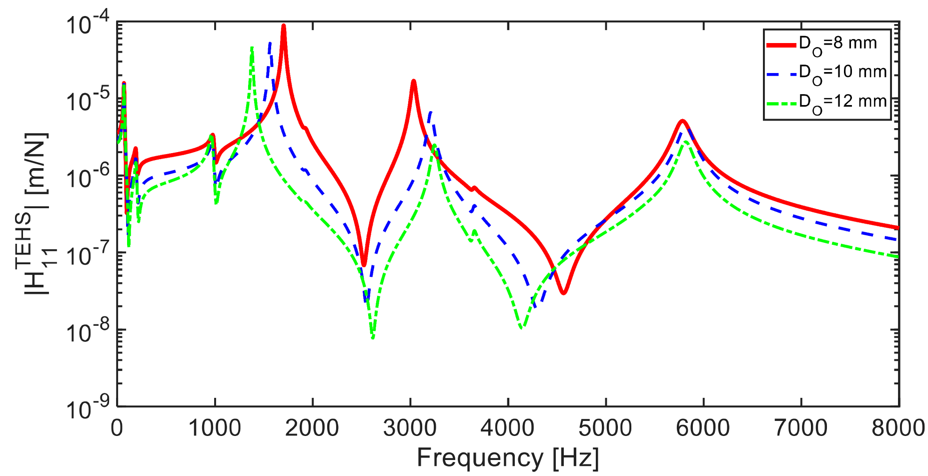

Figure 3.11 The effect of the diameter of the tool on the tool tip FRF

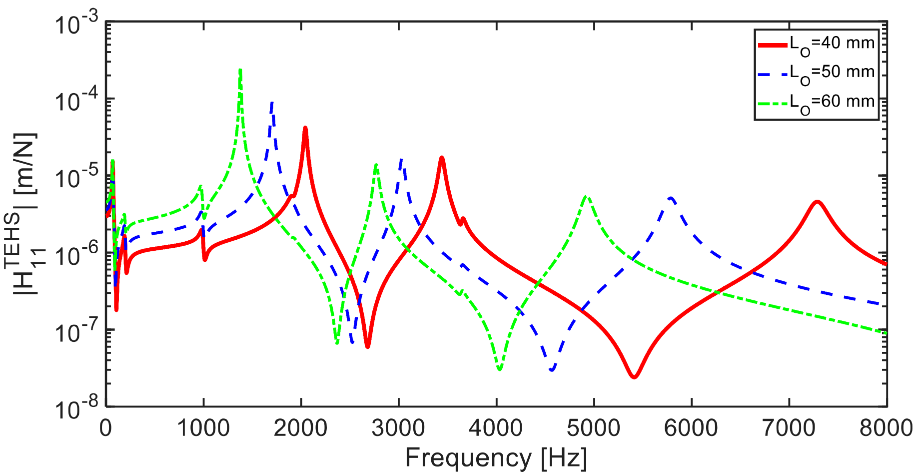

Figure 3.12 The effect of the overhang length of the tool on the tool tip FRF

CHAPTER 4

COMPARISON OF HOLDER EXTENSION DESIGNS IN FRF TUNING

4.1 Overview

As discussed in Chapter 3, an extension piece can be added between the holder and the tool instead of using long, slender and expensive tools in applications, e.g. in aerospace where it is often required to reach deep pockets. There are several holder extension designs readily used in the machining industry. Generally, the holder extension is a straight bar. However, these designs are mainly distinguished from each other with the clamping mechanism between the holder extension and the tool. The most common clamping mechanisms used are the collet and the shrink fit, as shown in Figure 4.1. The collet is usually a tapered element which is used to hold the tool by exerting a high clamping force when it is tightened. On the other hand, in the shrink fit, the interference fit between the holder extension inner diameter and the tool diameter is used to create a joint.

(a) Tool clamped to the holder extension with collet

(b) Tool clamped to the holder extension with shrink fit

Figure 4.1 Holder extension designs with different clamping mechanisms

There are also integrated holder extension designs, as shown in Figure 4.2. In these designs, there is a master holder into which a holder extension of any shape can be mounted with the help of a draw bolt. The tool is clamped to the extension piece with shrink fit.

Figure 4.2 Integrated holder extension design

In this Chapter, analytical case studies where different holder extension designs are optimized by creating dynamic interaction among the assembly components are conducted.

4.2 Case Study 1: Spindle System with Collet Holder and Tool Clamped to Holder Extension with Collet

In this case study, the dimensions and the material of the spindle, holder, holder extension and tool are the same as the ones in Section 2.5.3. However, the interface dynamics are assumed to be different from the ones in Section 2.5.3. The interface dynamics between the components used in Case Study 1 are given in Table. 4.1.

Table 4.1 Interface dynamics between the components for Case Study 1

	Spindle-holder Interface	Holder-holder extension Interface	Holder extension-tool Interface
Translational Stiffness [N/m]	5×10^7	2×10^7	0.75×10^7
Translational Damping [N.s/m]	50	10	10
Rotational Stiffness [N.m/rad]	1.5×10^6	1.5×10^6	1.5×10^6
Rotational Damping [N.s.m/rad]	170	10	10

Figure 4.3 shows the tool tip FRF of the TEHS assembly where the tool is clamped to the holder extension with the collet. The critical mode of the assembly is around 1700 Hz. The effective modes in the holder tip FRF are depicted in Figure 4.4. As it can be seen, the modes around 900 Hz, 1750 Hz, 3500 Hz and 5500 Hz at the holder tip can be used for FRF tuning.

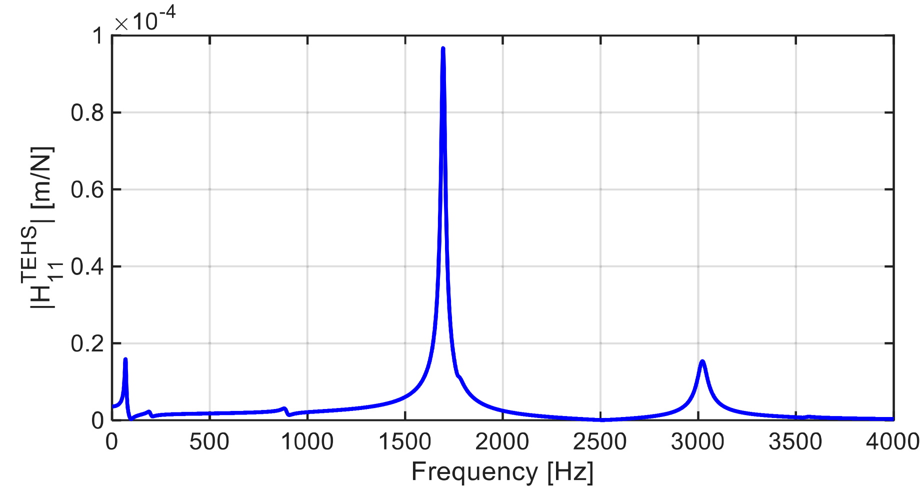

Figure 4.3 Tool tip FRF of the TEHS assembly with arbitrary holder extension length (40 mm) and arbitrary tool overhang length (50 mm) when the tool is clamped with collet

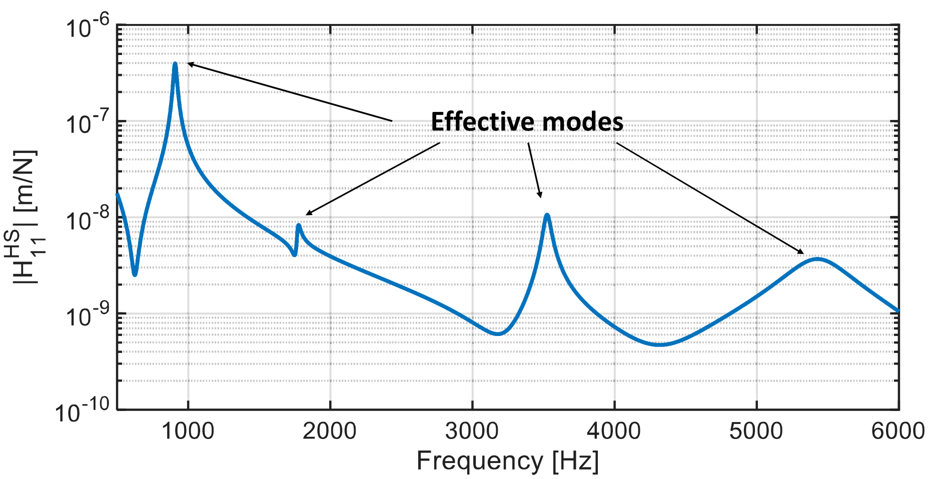

Figure 4.4 Effective modes in the holder tip FRF

4.2.1 Modification of Tool Tip FRF by Simultaneous Optimization of Holder Extension and Tool Overhang Length

The optimization problem is formulated as follows:

$$
\begin{aligned}
&\phi(L_E, L_O) = \max\left(\left|H_{11}^{TEHS}\right|\right) \\
&30mm \le L_E \le 60mm \\
&30mm \le L_O \le 60mm
\end{aligned}
\tag{4.1}
$$

Figure 4.5 shows the effect holder extension length and tool overhang length on the maximum amplitude of tool tip FRF. The optimum holder extension length and tool overhang length, which create dynamic absorber effect are found to be 56 mm and 32 mm, respectively.

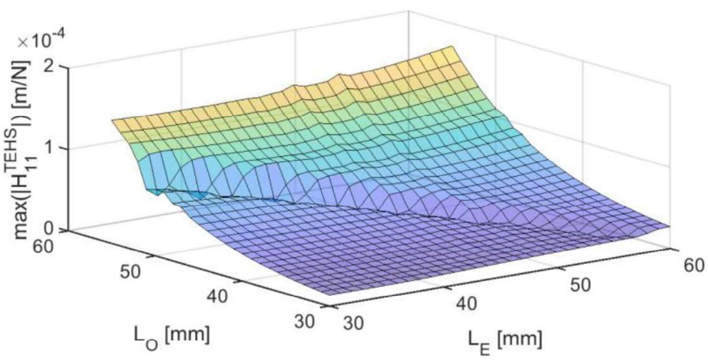

Figure 4.5 The effect of tool overhang length and holder extension length on the peak tool tip FRF when the tool is clamped with collet

The tuned tool tip FRF with simultaneous optimization of holder extension length (56 mm) and tool overhang length (32 mm) is depicted in Figure 4.6. This time, the first two natural frequencies of the cantilevered holder extension-tool subassembly are matched with the effective modes at 1750 Hz and 3500 Hz. This is an interesting result since the multi-mode FRF tuning is created similar to the multiple TMD systems where TMDs are tuned to different natural frequencies of the main system to control vibrations.

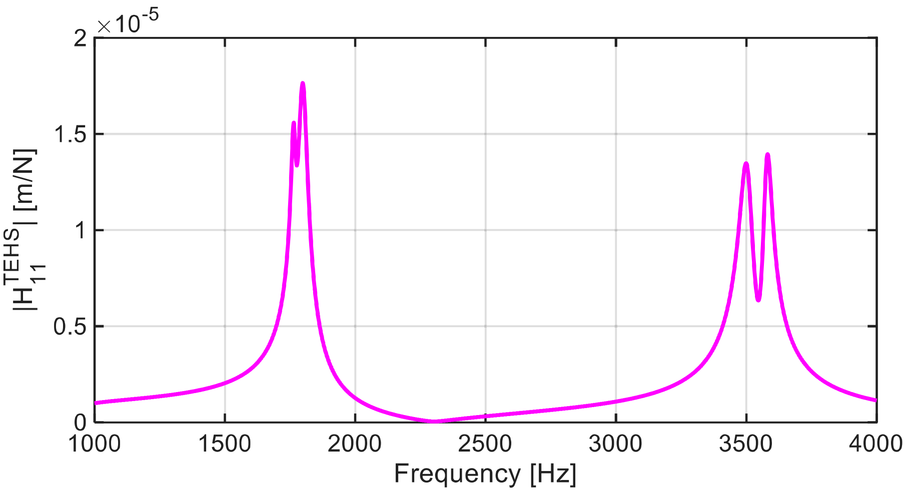

Figure 4.6 Tool tip FRF of the TEHS assembly with simultaneously optimized holder extension length (56 mm) and tool overhang length (32 mm) when the tool is clamped with collet

4.3 Case Study 2: Spindle System with Collet Holder and Tool Clamped to Holder Extension with Shrink Fit

The same TEHS assembly used in Case Study 1 is considered herein. However, this time, the tool is clamped to the holder extension with shrink fit while keeping all other parameters the same. Obviously, changing the clamping mechanism between the holder extension and the tool changes the interface dynamics of the holder extension-tool connection. Typical translational stiffness values for shrink fit connection in the literature are in the order of 10^8 N/m [14]. Figure 4.7 illustrates the tool tip FRF of the unmodified TEHS assembly when the translational stiffness at the holder extension- tool connection is taken as 10^8 N/m. The green dashed line shows the tool tip FRF of the same assembly when the interface at the holder extension-tool is assumed to be rigid, i.e., tool tip FRF of the assembly is calculated by rigid receptance coupling of the holder extension and the tool. Notice that, the tool tip FRF is almost the same when the holder extension-tool connection is rigid. Therefore, it can be concluded that shrink fit connection can be assumed to be a rigid connection.

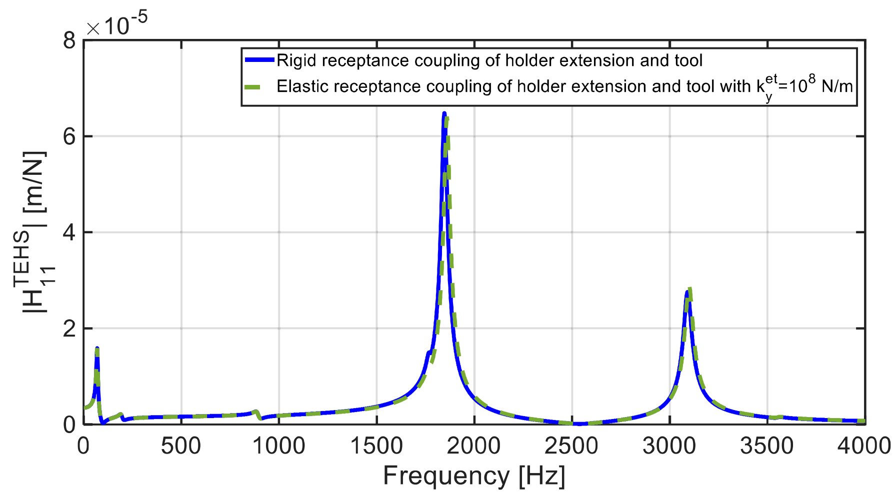

Figure 4.7 Tool tip FRF of the TEHS assembly with arbitrary holder extension length (40 mm) and tool overhang length (50 mm) when the tool is clamped with shrink fit

The calculated tool tip FRFs of the TEHS assemblies described in Case Study 1 and Case Study 2 are compared in Figure 4.8. As the holder extension-tool interface becomes rigid, the FRF at the critical mode of the assembly is reduced from 9.67×10^{-5} m/N to 6.27×10^{-5} m/N while the frequency is shifted from 1700 Hz to 1850 Hz.

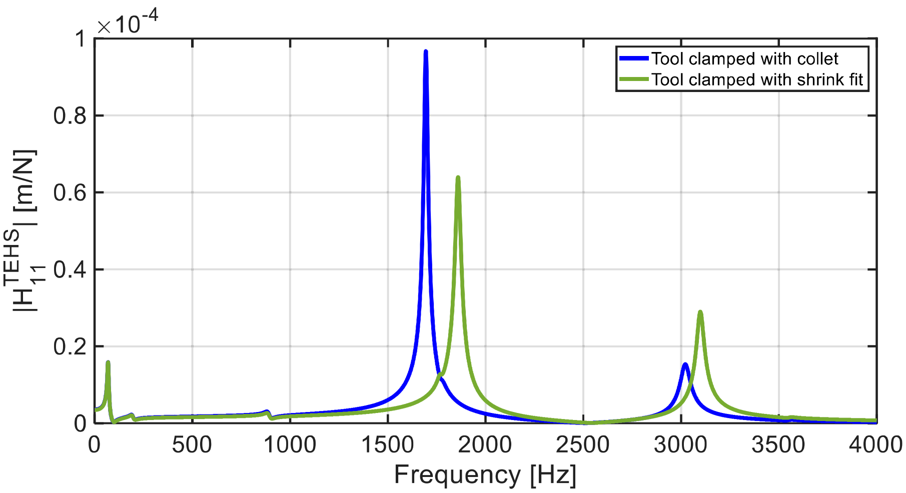

Figure 4.8 Comparison of tool tip FRFs of TEHS assemblies when the tool is clamped with collet and shrink fit

4.3.1 Modification of Tool Tip FRF by Simultaneous Optimization of Holder Extension and Tool Overhang Length

The optimization problem is formulated as follows:

$$\phi(L_E, L_O) = \max\left(\left|H_{11}^{TEHS}\right|\right) \tag{4.2}$$
$$30mm \le L_E \le 60mm$$
$$30mm \le L_O \le 60mm$$

The maximum amplitude of tool tip FRF for different holder extension length and tool overhang length combinations in the given ranges is depicted in Figure 4.9. The holder extension length and the tool overhang length combination, which created modal interaction, is found to be 49 mm and 41 mm, respectively. Figure 4.10 shows the tuned tool tip FRF of the optimized TEHS assembly. Interestingly, the second natural frequency of the cantilevered holder extension-tool subassembly is matched with the effective mode at 3500 Hz. This is due to the fact that, the second mode of the holder extension-tool subassembly dominates the critical mode of the TEHS assembly as discussed in Section 3.2.1.

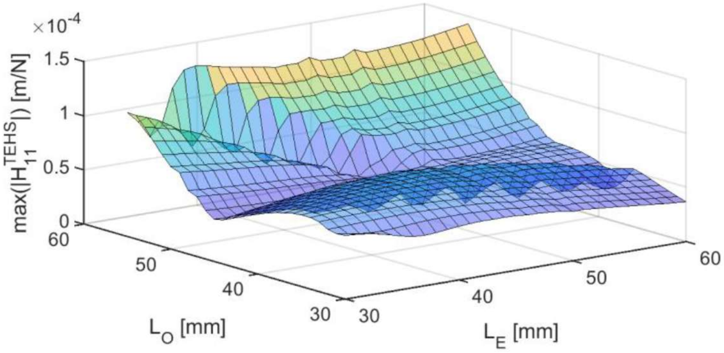

Figure 4.9 The effect of tool overhang length and holder extension length on the peak tool tip FRF when the tool is clamped with shrink fit

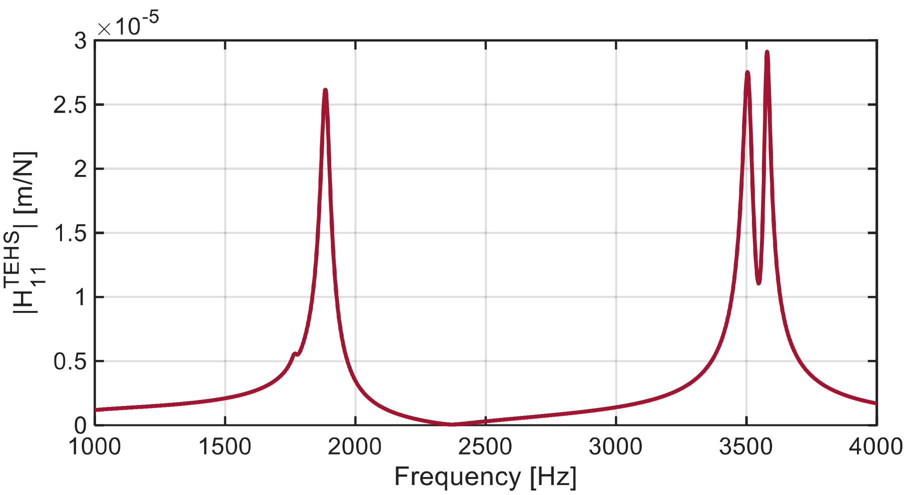

Figure 4.10 Tool tip FRF of the TEHS assembly with simultaneously optimized holder extension length (49 mm) and tool overhang length (41 mm)

Calculated tool tip FRFs of the optimized TEHS assembly for Case Study 1 and Case Study 2 are compared in Figure 4.11. The maximum amplitude of tool tip FRF of the tuned TEHS assembly is 1.8×10^{-5} m/N for Case Study 1 while it is 2.9×10^{-5} m/N for Case Study 2. Moreover, the effective lengths are 88 mm and 90 mm, respectively. Contrary to the intuition, the tuned tool tip FRF of the spindle system in which tool is clamped to holder extension with collet results in a dynamically stiffer system while the effective length remains almost the same. Therefore, it can be concluded that, the elastic connection at the holder extension-tool interface can be advantageous to suppress the peak tool tip FRF due to dynamic interaction in some applications.

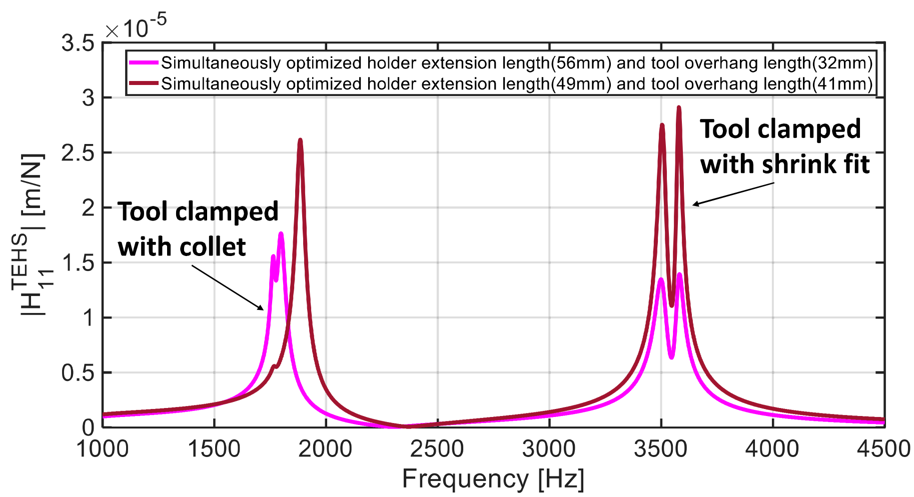

Figure 4.11 Comparison of tuned tool tip FRFs of TEHS assemblies when the tool is clamped with collet and shrink fit

Figure 4.12 shows the tool tip FRF of the assembly where the tool of 50 mm overhang length is clamped to the same spindle-holder subassembly described in Case Study 1. The interface dynamics between the holder and the tool is assumed to be the same as the one between the holder extension and the tool. The critical mode of the THS assembly is at 2250 Hz. The tool tip FRF is tuned to the effective mode at 3500 Hz when the tool overhang length is 35 mm.

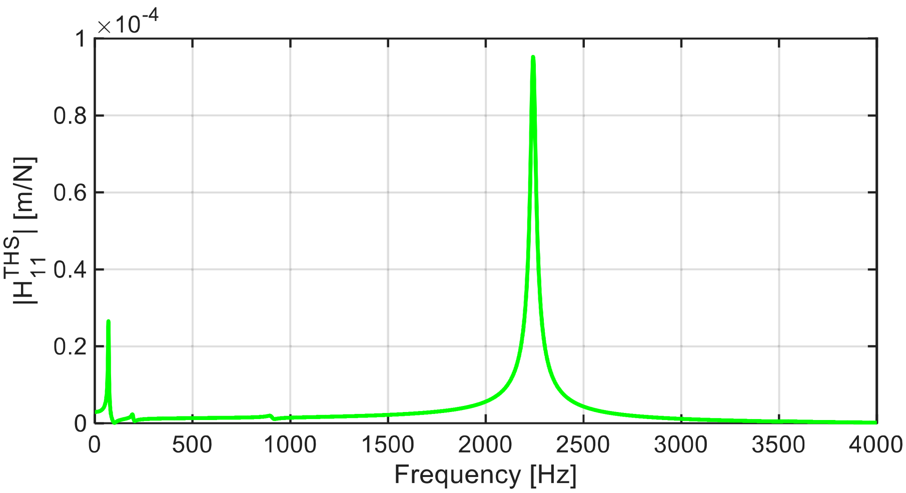

Figure 4.12 Tool tip FRF of the THS assembly with arbitrary tool overhang length (50 mm)

The tool tip FRFs of the THS assembly with tuned tool overhang length and TEHS assembly with simultaneously tuned holder extension length and tool overhang length in Case Study 1 are compared in Figure 4.13. The peak tool tip FRF of the THS assembly is decreased from 9.5×10^{-5} m/N to 1.3×10^{-5} m/N with the tool overhang length tuning. On the other hand, the peak tool tip FRF is 1.8×10^{-5} m/N for the tuned TEHS assembly where the tool is clamped with collet. Notice that, overall effective length is 88 mm for the tuned TEHS assembly while it is reduced to 35 mm for the tuned THS assembly. On the contrary, there is no remarkable difference in the peak tool tip FRF between the two tuned assemblies. Therefore, multi-component dimension tuning of the holder extension and the tool can be favorable in applications where it is not possible to shorten the tool overhang length.

Consider the optimization problem for the TEHS assembly given in Case Study 1 in which only the holder extension length is the variable while the overhang length of the tool is kept 50 mm. In this case, the dominant mode of the assembly is shifted to the effective mode at 1750 Hz when the holder extension length is 34 mm. The blue line in Figure 4.13 shows the tool tip FRF of the TEHS assembly with optimized holder extension length (34 mm) and an arbitrary tool overhang length (50 mm). The results show that the multi-component dimension optimization in TEHS assemblies is crucial in maximizing the TMD effect resulting in increased dynamic rigidity.

The tool tip FRF of the TEHS assembly with separately optimized holder extension length (34 mm) and tool overhang length (35 mm) is also depicted in Figure 4.13. In this case, the peak tool tip FRF is increased from 1.8×10^{-5} m/N to 2.07×10^{-5} m/N compared to that of the simultaneous optimization of the holder extension length and the tool overhang length. Conversely, the overall effective length is decreased from 89 mm to 69 mm. It can be concluded that, the dimensions of the holder extension and the tool should be optimized simultaneously to create dynamic interaction between the subassemblies and in turn to increase dynamic rigidity.

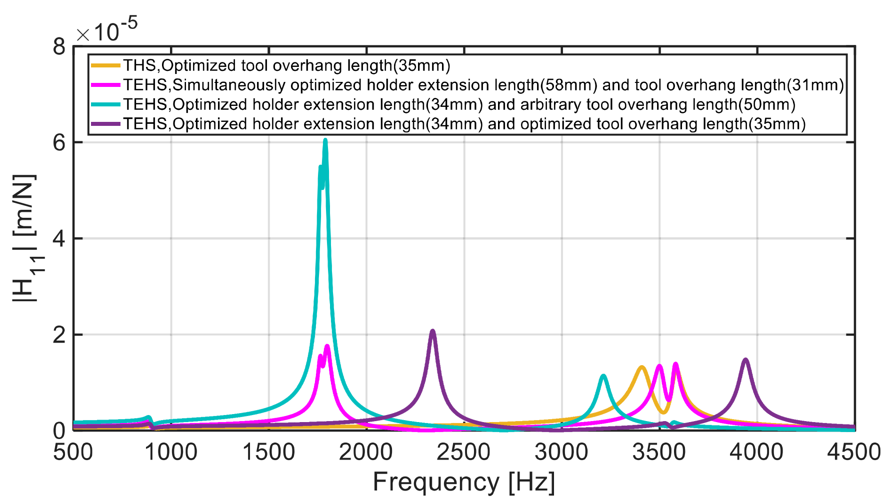

Figure 4.13 Comparison of tuned tool tip FRFs of THS and TEHS assemblies

4.4 Case Study 3: Spindle System with Integrated Holder Extension and Tool Clamped to Holder Extension with Shrink Fit

A typical spindle system with integrated holder extension is depicted in Figure 4.14. The master holder can be selected from readily available standard holder. On the contrary, it is possible to have custom made integrated holder extension designs. Therefore, the profile of the integrated holder extension can be optimized to create modal interaction among the assembly components. Additionally, as shown before, the overhang length of the tool can be adjusted as desired.

In this case study, the same spindle described in Case Study 1 and Case Study 2 is considered. Furthermore, it is assumed that the dimensions of the master holder are the same as the ones of the holder given in the previous case studies. For convenience, the interface dynamics at the spindle-holder connection and the holder-holder extension connection are assumed to be the same as the ones in Case Study 1 and Case Study 2. The end point receptances of the holder extension with a non-uniform profile is estimated by discretizing the holder extension into the n-segment beam as discussed in Section 2.2.1. The interface dynamics at the holder extension-tool connection is assumed to be rigid. Again, an 8 mm tool is clamped to the holder extension.

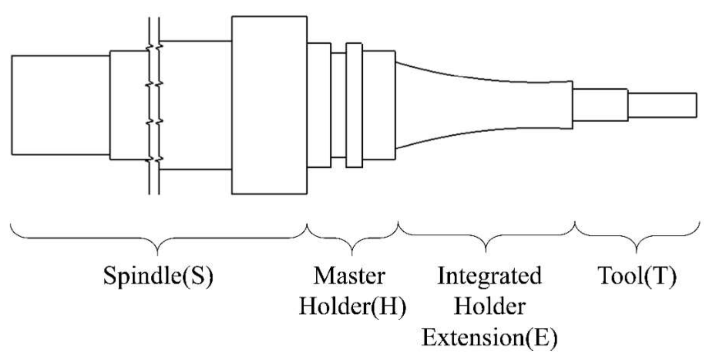

Figure 4.14 TEHS assembly with integrated holder extension

4.4.1 Modification of Tool Tip FRF by Simultaneous Optimization of Holder Extension and Tool Overhang Length while Holder Extension has a Parabolic Profile

In this case study, a parabolic profile is fitted to the holder extension. Figure 4.15 shows the profile of the integrated holder extension outside the holder. The diameter D_2 of the holder extension base is set to be 40 mm. The function of the profile of the holder extension is

$$f(x) = \frac{D_1}{2} + a \cdot x^2 \tag{4.3}$$

where

$$a = \frac{D_2 - D_1}{2 \cdot L_E^{\ 2}} \tag{4.4}$$

Therefore, the coefficient a is defined by the diameter D_1 of the holder extension tip and length L_E of the holder extension.

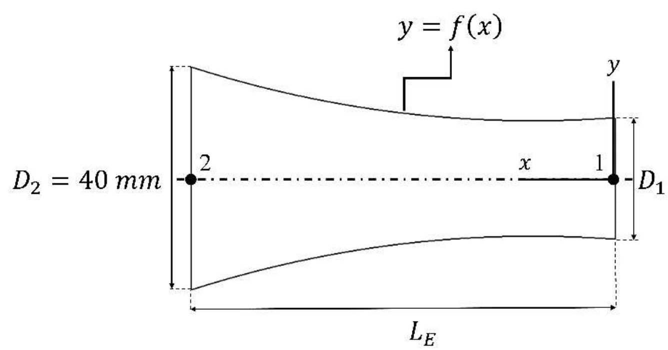

Figure 4.15 Profile of the holder extension outside the holder

The optimization problem is formulated as follows:

$$\begin{aligned} &\phi(L_E, L_O) = \max\left(\left|H_{11}^{TEHS}\right|\right) \\ &30mm \le L_E \le 60mm \\ &30mm \le L_O \le 60mm \end{aligned} \tag{4.5}$$

Figure 4.16, 4.17, and 4.18 show the effect of holder extension length and tool overhang length on the peak tool tip FRF when the diameter of the holder extension tip is 14 mm, 18 mm, and 24 mm, respectively.

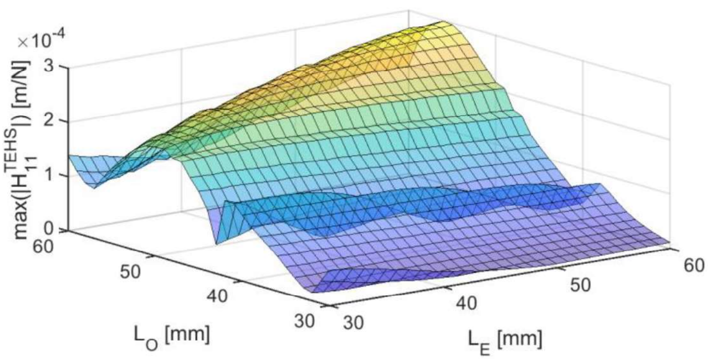

Figure 4.16 The effect of tool overhang length and holder extension length on the peak tool tip FRF when the diameter of the holder extension tip is 14 mm

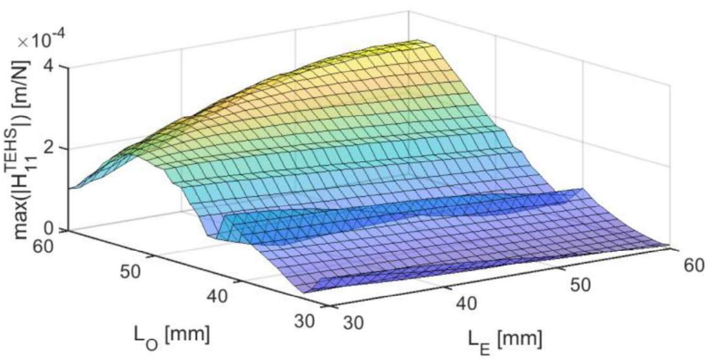

Figure 4.17 The effect of tool overhang length and holder extension length on the peak tool tip FRF when the diameter of the holder extension tip is 18 mm

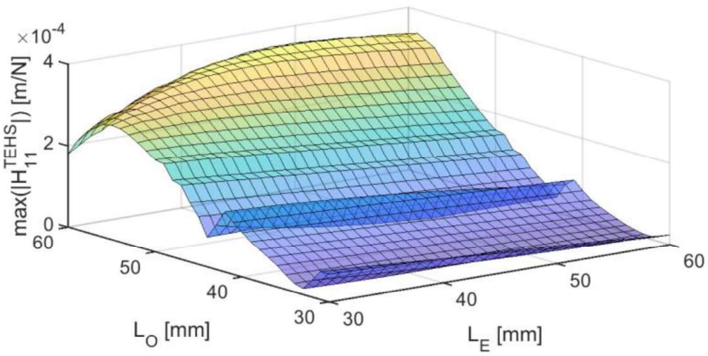

Figure 4.18 The effect of tool overhang length and holder extension length on the peak tool tip FRF when the diameter of the holder extension tip is 24 mm

The tuned holder extension and tool overhang lengths and corresponding peak tool tip FRFs for different tip diameter values of integrated holder extension with a parabolic profile are given in Table 4.2. The maximum amplitude of tool tip FRF is minimized when holder extension length and tool overhang length are 58 mm and 31 mm, respectively, while the diameter of the integrated holder extension tip with the parabolic profile is 18 mm.

Table 4.2 Optimum holder extension length and tool overhang length for different tip diameter values of integrated holder extension with a parabolic profile

	L_E [mm]	L_O [mm]	$\max\left(\left\|\mathrm{H}_{11}^{\mathrm{TEHS}}\right\|\right)$ [m/N]
D_1 = 14 mm	42	31	8.47×10^{-6}
D_1 = 18 mm	58	31	5.84×10^{-6}
D_1 = 24 mm	60	33	7.40×10^{-6}

The tool tip FRF with tuned holder extension profile and tool overhang length is depicted in Figure 4.19. This time, the second mode of the cantilevered holder extension-tool subassembly is matched with the effective mode at 5500 Hz. The maximum amplitude of tool tip FRF is decreased to 5.84×10^{-6} m/N due to dynamic interaction among the spindle-holder subassembly and the integrated holder extension-tool subassembly.

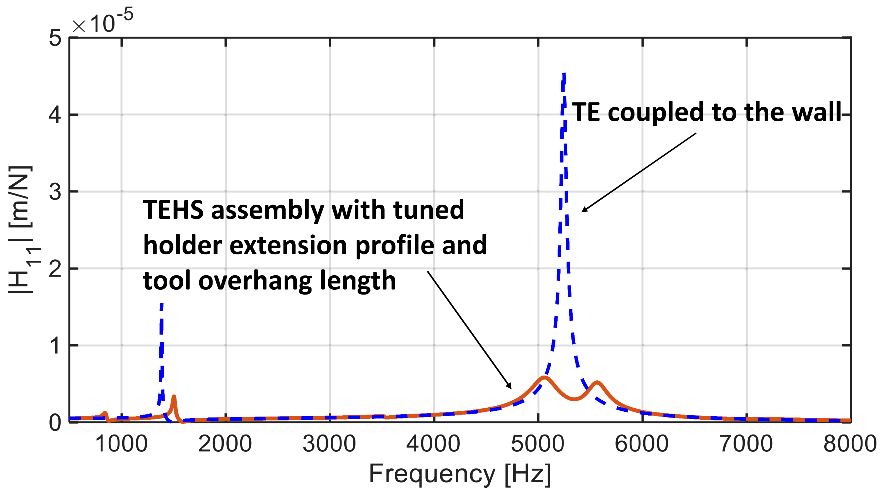

Figure 4.19 Tool tip FRF of the TEHS assembly with simultaneously optimized parabolic holder extension profile and tool overhang length

Calculated tool tip FRFs of the TEHS assembly for Case Study 1 and Case Study 3 are compared in Figure 4.20. The yellow line shows the tool tip FRF of the THS assembly with tuned tool overhang length (35 mm). As it can be seen from the Figure 4.20, the integrated holder extension design with a parabolic profile suppresses the critical mode of the assembly further compared to traditional holder extension design where the tool is clamped with collet while the effective length is almost the same for both cases. Furthermore, the damping capacity of the integrated holder extension-tool subassembly tuning is robust compared to tool overhang length tuning in a THS assembly. As a result, there is a great potential to suppress the dominant mode of the spindle systems with a custom design integrated holder extension-tool subassembly by creating dynamic absorber effect.

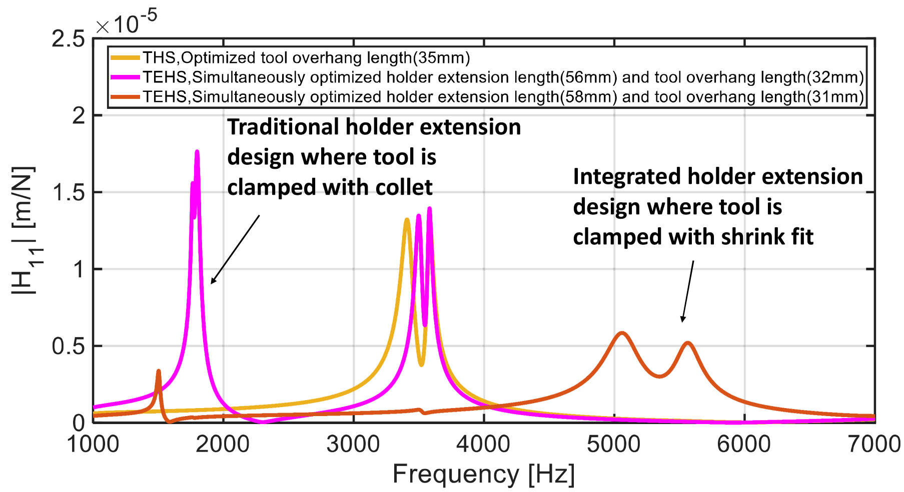

Figure 4.20 Comparison of tool tip FRFs with optimized component dimensions

The predicted stability lobe diagrams using tool tip FRFs with the optimized component dimensions are shown in Figure 4.21. The corresponding absolute stability limits are given in Table 4.3. Green line shows the stability limit of the THS assembly with an arbitrary tool overhang length. For the spindle-holder combination analyzed, by only tuning the overhang length of the tool, the stable MRR of a cutting process is increased more than seven times. Conversely, by addition of an optimized traditional holder extension between the holder and the tool and optimizing the overhang length of the tool, the stable MRR is increased more than five times compared to unmodified THS assembly. Therefore, it can be concluded that, depending on the dynamics of the structure, for a spindle-holder combination, tuning the dimensions of the traditional holder extension-tool subassembly may not always improve the absolute stability limit, and in turn the stable MRR of a cutting process, more than the case where just the overhang length of the tool is tuned. On the other hand, it can be seen that the stable MRR of a cutting process can be increased more than eighteen times by optimizing the parabolic profile of the integrated holder extension and the tool overhang length for a spindle-holder combination. As a result, the productivity of a cutting process can be enhanced further with a custom-made integrated holder extension design by using a parabolic profile and by adjusting the tool overhang length.

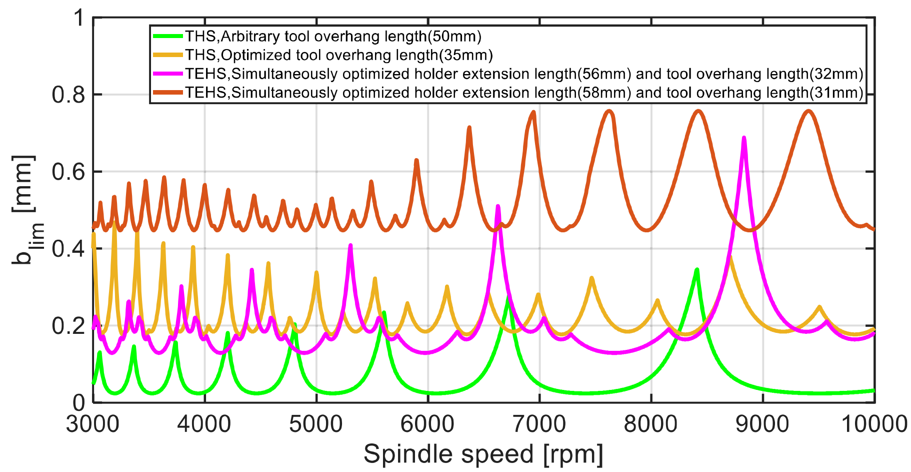

Figure 4.21 Stability lobe diagrams predicted using the tool tip FRFs with optimized component dimensions

Table 4.3 Comparison of absolute stability limits

	$b_{lim,abs}$ [mm]	Percent increase in $b_{lim,abs}$
THS, $L_O = 50$ mm	0.0240	-
THS, $L_O = 35$ mm	0.1771	637.9 %
TEHS, $L_O = 32$ mm, $L_E = 56$ mm	0.1290	437.5 %
TEHS, $L_O = 31$ mm, $L_E = 58$ mm	0.4471	1762.9%

CHAPTER 5

SUMMARY AND CONCLUSIONS

5.1 Summary of the Thesis

Chatter behavior of a cutting process strongly depends on the resulting FRF at the cutting point of a machine tool. In this thesis, an analytical optimization procedure of component dimensions is presented to suppress the dominant modal response at the tool tip. This is achieved by tuning the dimensions of the components to create TMD effect within the assembly resulting in increased dynamic rigidity. The FRF tuning methodology is based on matching the modes of the subassemblies of the structure. Consequently, the vibration energy of the most flexible part of the assembly is transferred to the rest of the structure. As a result, the peak final tool tip FRF is suppressed down to two smaller peaks which is a characteristic of TMD systems. Therefore, the stability limit and the stable area of a cutting process are increased.

The experimentally verified analytical model developed by Ertürk et al. [11] to calculate the tool tip FRF is used in calculating the tool tip FRF. In TEHS assemblies, the critical mode of the assembly is controlled by the holder extension-tool subassembly. Therefore, the analytical model developed Ertürk et al. [11] is used to investigate the effect of holder extension and tool design parameters on the resulting tool tip FRF. By using the analytical model, the optimum design parameters which minimize the peak tool tip FRF by imposing dynamic interaction are searched in the permissible ranges. Case studies are conducted to demonstrate reductions in the resulting peak tool tip FRFs and improvements in absolute stability limits. First, the tool overhang length is tuned to match the effective mode in the holder tip FRF in a THS assembly. An extension piece between the holder and the tool is added to the same spindle-holder combination. The length of the holder extension is optimized while keeping the overhang length of the tool the same. Later, both the lengths of the holder extension and the tool overhang are optimized simultaneously to match the dominant mode of the assembly to the chosen effective mode.

There are different holder extension designs involving various clamping mechanisms and shapes. In this thesis, their FRF tuning performances are compared by analytical case studies. The holder extension and the tool overhang lengths are optimized simultaneously while assuming the contact parameters representing the interface dynamics do not change. First, the lengths of the traditional holder extension where the tool is clamped using a collet and the tool overhang are tuned to create dynamic interaction. Secondly, the tuning capacity of the traditional holder extension where the tool is clamped with shrink fit is investigated. Finally, together with the overhang length of the tool, the profile of an integrated holder extension design is optimized to create TMD effect. It is shown that, the optimization of the dimensions of the integrated holder extension-tool subassembly provides the best result in FRF tuning method.

5.2 Conclusions

In this study, the peak FRF of the machine tool assembly is suppressed by design optimization of the holder extension-tool subassembly. Several case studies are conducted and some important observations are made. These are summarized below.

- Multi-component dimensional tuning achieved by optimizing the holder extension and the tool overhang lengths simultaneously suppresses the dominant modal contribution to the tool tip FRF remarkably with increased effective length. Therefore, design optimization of the holder extension-tool subassembly by creating TMD effect has a great potential in high speed machining applications, especially in aerospace, where it is needed to reach deep pockets during machining.

- In TEHS assemblies, the dominant mode of the assembly is controlled by the holder extension-tool subassembly. Therefore, resulting tool tip FRF can be modified as desired by changing the parameters of the holder extension and the tool.
- It is shown that, the dominant mode of the assembly can easily be modified by adjusting the length of the holder extension. On the other hand, holder extension starts to act as a mass as the diameter increases while keeping the length of the holder extension constant. It is also observed that, the profile of the holder extension can alter the critical mode of the assembly. Additionally, the desired tool tip FRF can be achieved by the proper selection of the diameter and the length of the tool.
- It is observed that the optimization of the holder extension and the tool dimensions separately gives misleading results. The results of the case studies show that the critical mode of the assembly is affected by the holder extension-tool subassembly as a whole. Therefore, the holder extension and the tool dimensions should be optimized simultaneously to create dynamic interaction between the spindle-holder subassembly and the holder extension-tool subassembly.
- It is not always possible to alter the contact parameters at the interfaces as desired in order to create/increase modal interaction. However, accurate identification of the contact parameters at these interfaces is crucial in semi-analytical design optimization of the holder extension-tool subassembly to tune the tool tip FRF.
- The results of the effect analysis suggest that, it is not possible to develop a generalized procedure to tune the critical mode of the assembly. The selected design parameters should be varied in simulations within the permissible ranges and the resulting tool tip FRF should be analyzed. Consequently, the optimum design parameters creating the maximum modal interaction to suppress the critical mode of the assembly are found.

- The shrink fit tool clamping is assumed to be a rigid connection. This assumption brings a convenience as the identification of the contact parameters at the holder extension-tool interface is not needed. Nonetheless, the elastic connection in the holder extension-tool interface can be beneficial in suppressing the resulting tool tip FRF by imposing modal interaction.
- In Section 4.3.1, the reductions in the resulting tool tip FRF in modified TEHS assembly is compared with the modified THS assembly where the overhang length of the tool is optimized. It can be concluded that, the tool overhang length tuning without addition of a holder extension can be robust in FRF reduction in some cases. This is due to the fact that, shortening the overhang length of the tool results in a dynamically stiffer system.
- It is shown that, the profile of the holder extension can alter the critical mode of the assembly. Therefore, the overhang length of the tool and the profile of an integrated holder extension design are optimized simultaneously to create TMD effect in Section 4.4.1. It is shown that, the profile optimization of the holder extension could maximize the dynamic rigidity.

5.3 Suggestions for Future Work

In this thesis, the implementation of a tuned holder extension-tool subassembly to a spindle-holder combination is studied for milling applications. Nonetheless, this procedure can be applied to boring and turning operations to increase the dynamic rigidity.

It can be recommended to study different shapes other than the parabolic profile in tuning the holder extension. Furthermore, different materials could also be used to manufacture optimum holder extension design. Besides, it is possible to manufacture bi-material holder extensions by using friction welding. Moreover, the shape of the holder extension and the spindle can also be optimized with the given FRF tuning methodology.

From the effect analysis, it has been shown that the contact parameters at the holder-holder extension and holder extension-tool interface can alter the dominant mode of the assembly. Therefore, in applications of the FRF tuning method, the contact parameters at the interfaces should be identified and used in the analytical model for predicting the resulting tool tip FRF and optimizing the component dimensions accordingly. Therefore, an experimental verification of the tuning method is needed. Furthermore, it is assumed that the contact parameters at these interfaces do not change while the design parameters of the holder extension-tool subassembly are varied in permissible ranges. This assumption is valid if the resulting optimum design is not drastic. On the other hand, as it is shown by Matthias et al. [43], the contact parameters at the holder-tool interface are sensitive to the changes in tool overhang length, tool diameter and clamping torque etc. In order to overcome these difficulties, the profile of the holder extension can be optimized by using structural modification methods if the holder extension and the tool overhang length are decided.

REFERENCES

[1] Munoa J. et al.,2016. Chatter suppression techniques in metal cutting, CIRP Annals 65(2), pp. 785-808.

[2] J. Tlusty, M. Polacek, 1963. The stability of machine tools against self-excited vibrations in machining, Proceedings of the ASME International Research in Production Engineering, pp. 465-474.

[3] H. Merrit, 1965. Theory of self-excited machine tool chatter, Transactions of ASME Journal of Engineering for Industry 87, pp. 447-454.

[4] Y. Altintas, E. Budak, 1995. Analytical prediction of stability lobes in milling, Annals of CIRP 44(1), pp. 357-362.

[5] E. Budak, Y. Altintas, 1998. Analytical prediction of chatter stability in milling part I: general formulation; part II: application to common milling systems, Transactions of ASME, Journal of Dynamic Systems, Measurement, and Control 120, pp. 22-365

[6] J. Tlusty, 2000. Manufacturing Processes and Equipment, Prentice Hall, Upper Saddle River, NJ.

[7] T. Schmitz, R. Donaldson, 2000. Predicting high-speed machining dynamics by substructure analysis, Annals of CIRP 49(1), pp. 303-308.

[8] T. Schmitz, M. Davies, M. Kennedy, 2001. Tool point frequency response prediction for high speed machining by RCSA, Journal of Manufacturing Science and Engineering 123, pp. 707-707.

[9] T. Schmitz, M. Davies, K. Medicus, J. Snyder, 2001. Improving high speed machining material removal rated by dynamic rapid analysis, Annals of CIRP 50(1), pp. 263-268.

[10] T. Schmitz, T. Burns, 2003. Receptance coupling for high speed dynamics prediction, Proceedings of 21st International Modal Analysis Conference, Kissimmee, FL.

[11] A. Ertürk, H.N. Özgüven, E. Budak, 2006. Analytical modeling of spindle-tool dynamics on machine tools using Timoshenko beam model and receptance coupling for prediction of tool point FRF, International Journal of Machine Tools and Manufacture 46(15), pp. 1901-1912.

[12] E. Budak, A. Ertürk, H.N. Özgüven, A modeling approach for analysis and improvement of spindle-holder-tool assembly dynamics, Annals of CIRP 55(1), pp. 369-372.

[13] O. Özşahin, E. Budak, H.N Özgüven, 2012. Analytical Modelling of Machine Tool Spindle Dynamics Under Operational Conditions, Proceedings of the 37th International MATADOR Conference, Manchester, UK.

[14] T. Schmitz, K. Powell, D. Won, G.S. Duncan, W.G. Sawyer, J.C. Ziegert, 2007. Shrink fit tool holder connection stiffness/damping modeling for frequency response prediction in milling, International Journal of Machine Tools and Manufacture 47, pp. 1368-1380.

[15] K. Ahmadi, H. Ahmadian, 2007. Modeling machine tool dynamics using a distributed parameter tool-holder joint interface, International Journal of Machine Tools and Manufacture 47, pp. 1916-1928.

[16] A. Ertürk, H.N. Özgüven, E. Budak, 2007. Effect analysis of bearing and interface dynamics on tool point FRF for chatter stability in machine tools by a new analytical model for spindle-tool assemblies, International Journal of Machine Tools and Manufacture 47(1), pp. 23-32.

[17] O. Özşahin, A. Ertürk, H.N. Özgüven, E. Budak, 2009. A closed form approach for identification of dynamical contact parameters in spindle-holder-tool assemblies, International Journal of Machine Tools and Manufacture 49(1), pp. 25-35.

[18] O. Özşahin, E. Budak, H.N. Özgüven, 2008. Estimation of dynamic contact parameters machine tool spindle-holder-tool assemblies using artificial neural networks, Proceedings of the 3rd International Conference on Manufacturing Engineering (ICMEN), pp. 131-144.

[19] P. Watts, 1883. On a method of reducing the rolling of ships at sea, Transactions of the Institution of Naval Architects, 24, pp. 165-190.

[20] H. Frahm, 1909. Device for damping vibrations of bodies. US Patent No: 989958.

[21] J. Ormondroyd and J.P. Den Hartog, 1928. Theory of dynamic vibration absorber, Transactions of the American Society of Mechanical Engineers, 50, pp. 87-106.

[22] J.P Den Hartog, 1956. Mechanical Vibrations, McGraw-Hill Book Company.

[23] S.E. Randall, D.M. Halsted, D.L. Taylor, 1981. Optimum vibration absorbers for linear damped system, ASME Journal of Mechanical Design, 103, pp. 908-913.

[24] Y.S. Tarng, Y.J. Kao, E.C. Lee, 2000. Chatter suppression in turning operations with a tuned vibration absorber, Journal of Materials Processing Technology 105(1), pp.55-60.

[25] M.H. Miguélez, L. Rubio, J.A. Loya, J. Fernándes-Sáez, 2010. Improvement of chatter stability in boring operations with passive vibration absorbers, International Journal of Mechanical Sciences 52(10), pp. 1376-1384.

[26] Y. Yang, J. Munoa, Y. Altintas, 2010. Optimization of multiple tuned mass dampes to suppress machine tool chatter, International Journal of Machine Tools and Manufacture 50, pp. 834-842.

[27] A. Rashid, C.M. Nicolescu, 2008. Design and implementation of tuned viscoelastic dampers for vibration control in milling, International Journal of Machine Tools and Manufacture 48, pp. 1036-1053.

[28] Y. Yang, W. Dai, Q. Liu, 2015. Design and implementation of two-degree-of-freedom tuned mass damper in milling vibration mitigation, Journal of Sound and Vibration, 335, pp. 78-88.

[29] M. Wang, 2011. Feasibility study of nonlinear tuned mass damper for machining chatter suppression, Journal of Sound and Vibration 330(9), pp. 1917-1930.

[30] M. Wang, T. Zan, Y. Yang, R. Fei, 2010. Design and implementation of nonlinear TMD for chatter suppression: An application to turning processes, International Journal of Machine Tools and Manufacture 50, pp. 474-479.

[31] J. Tlusty, S. Smith, W.R. Winfough, 1996. Techniques for the Use of Long Slender End Mills in High-speed Milling, CIRP Annals 45(1), pp. 393-396.

[32] M. Davies, B. Dutterer, J. Pratt, A. Schaut, 1998. On the dynamics of high-speed milling with long, slender endmills, Annals of the CIRP 47(1), pp. 55-60.

[33] S. Smith, W. Winfough, J. Harley, 1998. The effect of tool length on stable metal removal rate in high-speed milling, Annals of the CIRP 47(1), pp. 307-310.

[34] G.S. Duncan, M.F. Tummond, T.L. Schmitz, 2005. An investigation of the dynamic absorber effect in high-speed machining, International Journal of Machine Tools and Manufacture 45, pp. 497-507.

[35] A. Ertürk, E. Budak, H.N. Özgüven, 2007. Selection of design and operational parameters in spindle-holder-tool assemblies for maximum chatter stability by using a new analytical model, International Journal of Machine Tools and Manufacture 47(9), pp. 1401-1409.

[36] Y. Mohammedi, M. Azvar, E. Budak, 2018. Suppressing vibration modes of spindle-holder-tool assembly through FRF modification for enhanced chatter stability, CIRP Annals 67(1), pp. 397-400.

[37] S.P. Timoshenko, 1953. History of Strength of Materials, McGraw-Hill Book Company, New York.

[38] S.P. Timoshenko, 1921. On the correction for shear of the differential equation for transverse vibrations of prismatic bars, Philosophical Magazine 41, pp. 744-746.

[39] S.P. Timoshenko, 1922. On the transverse vibrations of bars of uniform cross-section, Philosophical Magazine 43, pp. 125-131.

[40] J.D. Aristizabal-Ochoa, 2004. Timoshenko beam-column with generalized end conditions and nonclassical modes of vibration of shear beams, Journal of Engineering Mechanics 130(10), pp 1151-1159.

[41] H.N. Özgüven, 1990. Structural modifications using frequency response functions, Mechanical Systems and Signal Processing 4(1), pp. 53-63.

[42] R.G. Parker, L.R. Rardin, 1988. Discrete Optimization, Academic Press.

[43] W. Matthias, O. Özşahin, Y. Altıntaş, B. Denkena, 2016. Receptance coupling based algorithm for the identification of contact parameters at holder-tool interface, CIRP Journal of Manufacturing Science and Technology 13, pp. 37-45.